

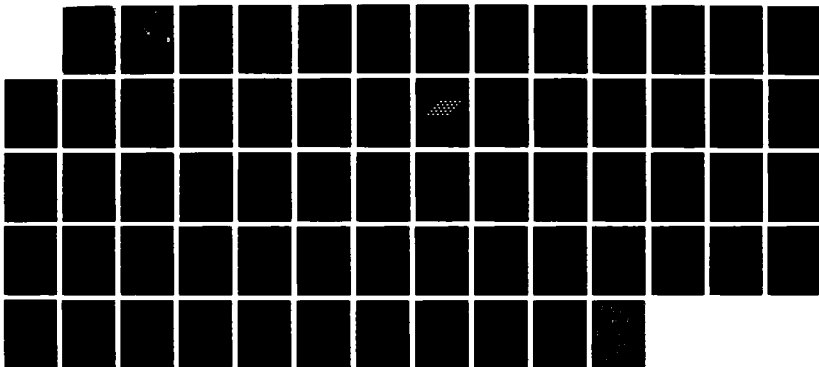
AD-R190 000

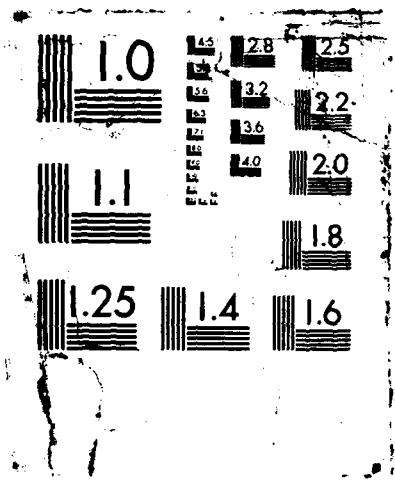
TARGET LOCALIZATION IN AN INHOMOGENEOUS MEDIUM(U) NAVAL 1/1
POSTGRADUATE SCHOOL MONTEREY CA H D BUDNEY DEC 87

UNCLASSIFIED

F/G 17/1

NL





AD-A190 008

DTIC FILE COPY

②

NAVAL POSTGRADUATE SCHOOL

Monterey, California



DTIC
ELECTE
MAR 04 1988
S & E D

THESIS

TARGET LOCALIZATION IN AN INHOMOGENEOUS
MEDIUM

by

Michael D. Budney

December 1987

Thesis Advisor

L. J. Ziomek

Approved for public release; distribution is unlimited.

88 3 01 015

UNCLASSIFIED

SECURITY CLASSIFICATION OF THIS PAGE

A190008

REPORT DOCUMENTATION PAGE

1a REPORT SECURITY CLASSIFICATION UNCLASSIFIED		1b RESTRICTIVE MARKINGS	
2a SECURITY CLASSIFICATION AUTHORITY		3 DISTRIBUTION/AVAILABILITY OF REPORT Approved for public release; distribution is unlimited	
2b DECLASSIFICATION/DOWNGRADING SCHEDULE			
4. PERFORMING ORGANIZATION REPORT NUMBER(S)		5 MONITORING ORGANIZATION REPORT NUMBER(S)	
6a NAME OF PERFORMING ORGANIZATION Naval Postgraduate School	6b OFFICE SYMBOL (if applicable) 62	7a NAME OF MONITORING ORGANIZATION Naval Postgraduate School	
6c. ADDRESS (City, State, and ZIP Code) Monterey, California 93943-5000		7b ADDRESS (City, State, and ZIP Code) Monterey, California 93943-5000	
8a. NAME OF FUNDING / SPONSORING ORGANIZATION	8b OFFICE SYMBOL (if applicable)	9 PROCUREMENT INSTRUMENT IDENTIFICATION NUMBER	
8c. ADDRESS (City, State, and ZIP Code)		10 SOURCE OF FUNDING NUMBERS	
		PROGRAM ELEMENT NO.	PROJECT NO.
		TASK NO.	WORK UNIT ACCESSION NO.
11 TITLE (Include Security Classification) Target Localization in an Inhomogeneous Medium (UNCLASSIFIED)			
12 PERSONAL AUTHOR(S) Michael D. Budney			
13a. TYPE OF REPORT Master's Thesis	13b TIME COVERED FROM _____ TO _____	14. DATE OF REPORT (Year, Month, Day) 1987 December	15 PAGE COUNT 64
16. SUPPLEMENTARY NOTATION			
17 COSATI CODES		18 SUBJECT TERMS (Continue on reverse if necessary and identify by block number) Sonar; Model-Based; Signal Processing; Planar Array; Ray Acoustics	
FIELD	GROUP SUB-GROUP		
19 ABSTRACT (Continue on reverse if necessary and identify by block number) A computer algorithm was developed to determine if an acoustic transmitter can be localized based on estimates of local angles of arrival of acoustic signals incident upon a receive planar sonar array, knowledge of the deterministic effects of the ocean on sound propagation, and local sound-speed profiles of the ocean. The algorithm was designed to determine azimuthal and elevation/depression angles to the transmitter as well as computing the depth, range, cross range, and line-of-sight range separations between the transmitter and the receive array. The algorithm utilizes ray acoustics and model-based phase weights to determine the transmitter's location relative to the receive array's position. As written, the algorithm is capable of solving localization problems in which the transmitter and receiver are in the same gradient of the local sound-speed profile, provided that the range			
20 DISTRIBUTION/AVAILABILITY OF ABSTRACT <input checked="" type="checkbox"/> UNCLASSIFIED/UNLIMITED <input type="checkbox"/> SAME AS RPT <input type="checkbox"/> DTIC USERS		21 ABSTRACT SECURITY CLASSIFICATION UNCLASSIFIED	
22a NAME OF RESPONSIBLE INDIVIDUAL L. J. Ziomek		22b TELEPHONE (Include Area Code) (408)-646-3206	22c OFFICE SYMBOL 622m

19. Abstract continued

from transmitter to receiver is not so great that the acoustic signal passes through a turning point prior to reaching the receive array. The results indicate that the method proposed is viable for the class of problems for which it was designed, and accuracies on the order of 0.1 meters are obtained for line-of-sight ranges on the order of several kilometers. The angles calculated by the algorithm are all accurate to within 0.005 degrees.

Approved for public release; distribution is unlimited.

Target Localization in an Inhomogeneous Medium

by

Michael D. Budney
Lieutenant, United States Navy
B.S., U.S. Naval Academy, 1980



Submitted in partial fulfillment of the requirements for the degree of

MASTER OF SCIENCE IN ELECTRICAL ENGINEERING

from the

NAVAL POSTGRADUATE SCHOOL
December 1987

Accession For	
NTIS GRA&I	<input checked="" type="checkbox"/>
DTIC TAB	<input type="checkbox"/>
Unannounced	<input type="checkbox"/>
Justification	
By _____	
Distribution/	
Availability Codes	
Dist	Avail and/or Special
A-1	

Author:

Michael S. Budney
Michael D. Budney

Approved by:

Lawrence J. Ziemeck
L.J. Ziemeck, Thesis Advisor

J.P. Powers
J.P. Powers, Second Reader

J.P. Powers
J.P. Powers, Chairman,
Department of Electrical and Computer Engineering

Gordon E. Schacher
Gordon E. Schacher,
Dean of Science and Engineering

ABSTRACT

A computer algorithm was developed to determine if an acoustic transmitter can be localized based on estimates of local angles of arrival of acoustic signals incident upon a receive planar sonar array, knowledge of the deterministic effects of the ocean on sound propagation, and local sound-speed profiles of the ocean. The algorithm was designed to determine azimuthal and elevation/depression angles to the transmitter as well as computing the depth, range, cross range, and line-of-sight range separations between the transmitter and the receive array. The algorithm utilizes ray acoustics and model-based phase weights to determine the transmitter's location relative to the receive array's position. As written, the algorithm is capable of solving localization problems in which the transmitter and receiver are in the same gradient of the local sound-speed profile, provided that the range from transmitter to receiver is not so great that the acoustic signal passes through a turning point prior to reaching the receive array. The results indicate that the method proposed is viable for the class of problems for which it was designed, and accuracies on the order of 0.1 meters are obtained for line-of-sight ranges on the order of several kilometers. The angles calculated by the algorithm are all accurate to within 0.005 degrees.

TABLE OF CONTENTS

I.	INTRODUCTION	9
II.	THEORY	12
	A. PROBLEM OVERVIEW AND GEOMETRY	12
	B. TRANSMITTER LOCALIZATION THEORY	14
	C. LIMITATIONS OF RAY ACOUSTICS SOLUTION	32
	1. Turning Points	32
	2. Changes in Sound-Speed Profile	35
	3. Validity of Model-Based Phase Weights	35
	4. Depth Separation of Zero Meters	37
III.	COMPUTER IMPLEMENTATION OF LOCALIZATION THEORY	38
	A. PROGRAM DESCRIPTION	38
	1. Program LOCATE	38
	2. Subprogram PLOTTER	44
	B. ALGORITHM VALIDATION	50
	1. Generation of Received Signals	50
	2. Test Case Results	50
IV.	CONCLUSIONS AND RECOMMENDATIONS	60
	LIST OF REFERENCES	62
	INITIAL DISTRIBUTION LIST	63

LIST OF TABLES

1. DEPTH AND RANGE TO TURNING POINTS FOR A POSITIVE GRADIENT	34
2. DEPTH AND RANGE TO TURNING POINTS FOR A NEGATIVE GRADIENT	35
3. LOCATE VERSUS TRUE GEOMETRY (GEOMETRY 1)	52
4. LOCATE VERSUS TRUE GEOMETRY (GEOMETRY 2)	53
5. LOCATE VERSUS TRUE GEOMETRY (GEOMETRY 3)	54
6. LOCATE VERSUS TRUE GEOMETRY (GEOMETRY 4)	55
7. DOUBLE PRECISION VERSUS SINGLE PRECISION RESULTS	59

LIST OF FIGURES

2.1	System Geometry	13
2.2	Typical Sound-Speed Profile	16
2.3	Receive Planar Array Geometry	19
2.4	Topview of Geometry	31
2.5	Turning Point Ambiguity	33
2.6	Changing Sound-Speed Gradient	36
3.1	Elevation/Depression Angle	39
3.2	Azimuthal Angle	40
3.3	Program LOCATE Flowchart	41
3.4	Program LOCATE Flowchart	42
3.5	F(x,y) for Geometry 1	45
3.6	F(x,y) for Geometry 2	46
3.7	F(x,y) for Geometry 3	47
3.8	F(x,y) for Geometry 4	48
3.9	Subprogram PLOTTER Flowchart	49
3.10	Error in RLOS as a Function of Depth Separation	56
3.11	Error in RLOS as a function of Transmission Angle and/or Depth Separation	57
3.12	Sine and Cosine for 0 to 90 Degrees	58

ACKNOWLEDGEMENTS

The author would like to thank Professor L. J. Ziomek for his assistance and patience during the course of this research.

I would also like to thank my wife, Susan, for her encouragement and support during the many hours that this work required. None of this would have been possible without her.

I. INTRODUCTION

This thesis constitutes one part of a long range project to develop new sonar signal processing algorithms capable of rapidly solving sonar localization problems. At present, the solution of the sonar fire control problem can require a considerably longer time than that required for most other types of fire control problems. The long time required to achieve a solution can cause a significant degradation in a ship's ability to avoid counterdetection, due to continuously decreasing range to the target during problem solution. A sonar system capable of rapid target localization without requiring own ship's maneuvers would greatly enhance the capabilities of our ships, and allow for weapon firings at longer ranges.

The research question investigated in this thesis is whether or not it is possible to develop an algorithm which utilizes estimates of the local angles of arrival of acoustic signals incident upon a planar sonar array, knowledge of the deterministic effects of the ocean medium on sound propagation, and local sound-speed profiles of the ocean, to locate an acoustic transmitter, both in azimuthal angle and elevation/depression angle. In addition the model-based localization algorithm (hereafter referred to as the 'localization algorithm') was designed to provide the range, depth, cross range, and line-of-sight range between the acoustic transmitter and the receive array.

Ray acoustics provides methods of determining ranges and propagation angles for transmission of acoustic signals in inhomogeneous media [Ref. 1: sect. 6.2]. The deterministic effects of the inhomogeneous ocean medium on acoustic signals are well known. From a transmitter in a known position, it is possible to develop ray traces that illustrate the propagation of acoustic signals through the ocean medium. The intent here is to use this knowledge of sound propagation to find the transmitter's location based on the estimated angles of arrival at a receive array. The estimates of the local angles of arrival are obtained from a frequency domain adaptive beamforming algorithm developed by Ziomek and Chan [Ref. 2]. This algorithm performs frequency domain adaptive beamforming for planar sonar arrays using a modified complex LMS adaptive algorithm. The algorithm generates estimates of the local angles of arrival, namely, the azimuthal and elevation depression angles, of incoming acoustic signals.

However, in a real ocean environment, these local angles of arrival do not reflect the true line-of-sight angles to the target.

The localization algorithm uses the angle-of-arrival estimates, plus typical sound-speed profiles that are normally available to ships. In addition, it was found that one more piece of information is required to localize the target. This information is a model-based phase weight which is part of a model-based signal processing algorithm developed by Ziomek and Blount [Ref. 3]. These phase weights are used to "correct for deterministic, ocean medium, phase effects due to ray bending as a signal propagates in the inhomogeneous ocean medium whose index of refraction (sound-speed profile) is a function of depth." [Ref. 3] The phase weights were originally developed as part of an underwater acoustic communication problem in which receiver and transmitter locations were known. The form of the phase weights used will be presented in Chapter II.

For the problem investigated in this thesis, transmitter location is *unknown a priori* and, therefore, the model-based phase weights cannot be determined in exactly the same manner as was done in the algorithm developed by Ziomek and Blount [Ref. 3]. The usefulness of the localization algorithm developed in this thesis is based on the availability of the model-based phase weights. The research done here is a feasibility study of the ability to localize an acoustic transmitter *if* the phase weights were available. The development of an algorithm to generate the model-based phase weights was not the subject of this research.

The localization algorithm is limited to solving a particular class of problems. The localization algorithm is designed to accommodate vertical variations in sound-speed profile or, sound-speed profiles that are functions of depth only. Horizontal or range variations in sound-speed profile were not examined in this initial study because they constitute only a relatively small portion of ocean areas. Additionally, the transmitter and receiver are assumed to both be within the same sound-speed gradient. Finally, all case studies were conducted based on the assumption that the receiver was in close enough proximity to the transmitter so that the acoustic signal had not passed through a turning point prior to reaching the receiver. A turning point is defined as the point along a ray path at which the angle of propagation is 90 degrees with respect to the positive Y, or depth, axis. These three restrictions were necessary to limit the scope of the initial study to a size that would allow for a complete verification of the localization technique proposed, in the time allotted for the study.

Chapter II describes the theory used to develop the localization algorithm. An overview of the problem and its geometry is presented, and then the computations leading to the algorithm are discussed. Finally, the limitations of the algorithm are presented.

Chapter III consists of the computer simulation results and an explanation of the implementation of the theory in a computer algorithm. The output from the localization algorithm is compared to the known geometry, and a comparison of double precision versus single precision results is included. Additionally, the program is investigated to determine if errors develop as a function of the transmission angle and/or depth separation. As will be shown in Chapter II, the roots of a fourth-order polynomial must be determined to find the angle of transmission at the source. The roots for the fourth-order polynomial are found through use of an International Mathematical Subroutine Library (IMSL) subroutine and are verified by comparison with graphs of the function. These graphs also assist in determining the correct root to use during problem solution.

In Chapter IV, conclusions and recommendations are presented.

II. THEORY

A. PROBLEM OVERVIEW AND GEOMETRY

Traditionally, the localization of acoustic transmitters by ships has been carried out by obtaining many lines of bearing to the transmitter, and comparing these with own ship's motion to develop a geographic picture of the transmitter's motion. This method is time consuming and usually very lacking in terms of accuracy. Due to the nature of the deterministic effects of the ocean medium, a great deal of information is contained in the angles at which acoustic energy arrives at the receiver. Extraction of this information from the local angles of arrival, while not a simple task in of itself, would greatly simplify the problem of target localization.

As a first step in exploiting the information contained within the local angles of arrival, a geometry must be assumed for the problem. Figure 2.1 illustrates the general three-dimensional geometry used in the development of the method of target localization presented here.

From Figure 2.1 the following definitions are apparent:

- x_0, y_0, z_0 rectangular coordinates of the transmitter in meters.
- x_R, y_R, z_R rectangular coordinates of the center of the receive planar array in meters.
- $\Delta X, \Delta Y, \Delta Z$ cross range, depth, and Z coordinate separations, respectively, in meters between the transmitter and the receive array, where:
 - $\Delta X = x_R - x_0$
 - $\Delta Y = y_R - y_0$
 - $\Delta Z = z_R - z_0$
- ΔR polar radial distance in meters from the transmitter to the receive array.
Note: $\Delta R^2 = \Delta X^2 + \Delta Z^2$
- HDLTR polar radial distance in meters that a ray would travel in a homogeneous medium (constant sound-speed profile) between depths y_0 and y_R based on an angle of transmission of $\beta(y_0)$.
- HDLTX, HDLTZ distances in the X and Z directions, respectively, that a ray would travel in a homogeneous medium between depths y_0 and y_R based on an angle of transmission of $\beta(y_0)$.
- HRLOS line-of-sight range that a ray would travel in a homogeneous medium between depths y_0 and y_R based on an angle of transmission of $\beta(y_0)$.

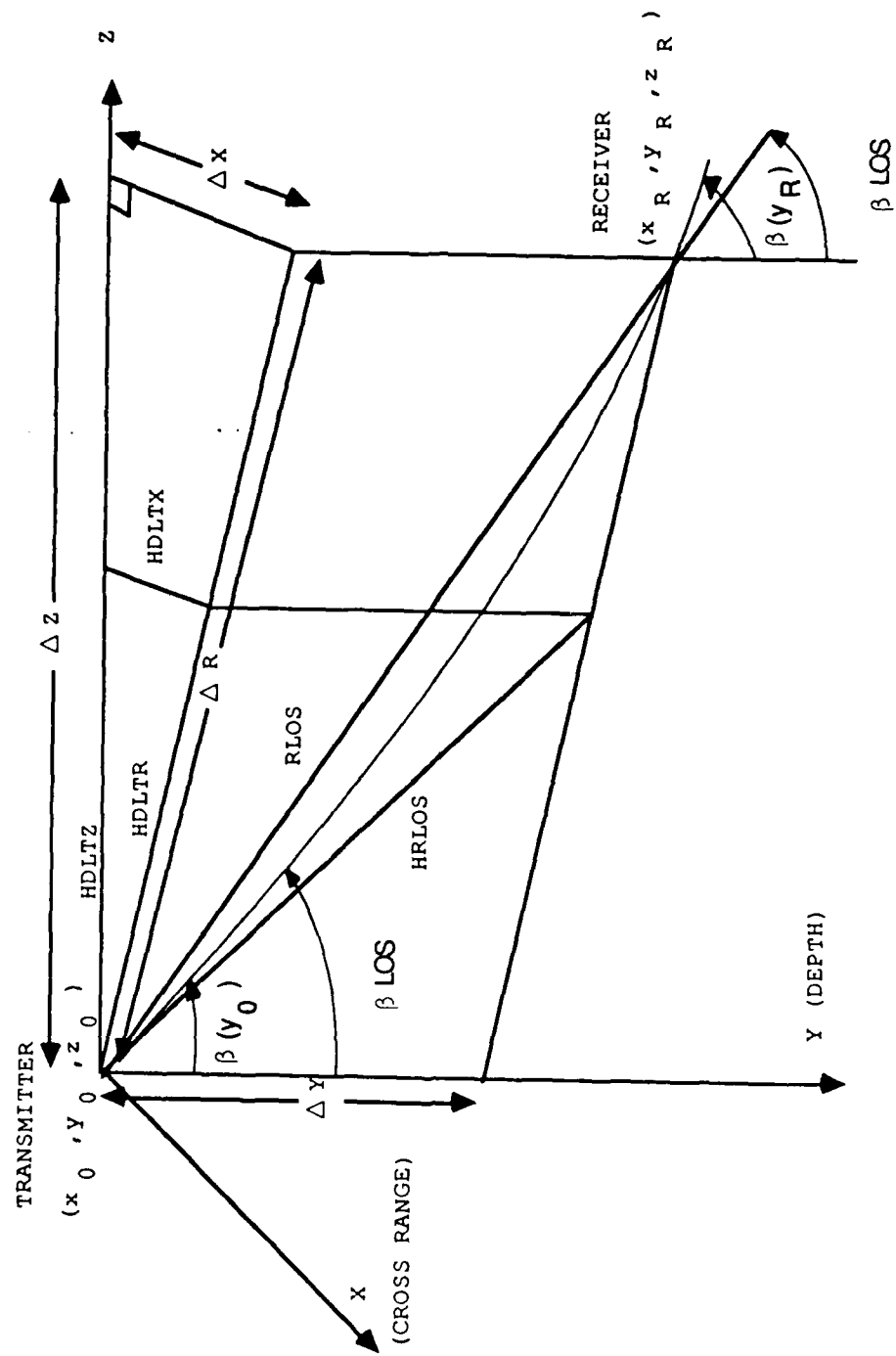


Figure 2.1 System Geometry.

Note: $HRLOS^2 = HDLTX^2 + \Delta Y^2 + HDLTZ^2$.

- RLOS line-of-sight range between the transmitter and the center of the receive array.
Note: $RLOS^2 = \Delta X^2 + \Delta Y^2 + \Delta Z^2$
- $\beta(y_0)$ initial angle of propagation (angle of transmission), measured with respect to the positive Y axis, of the acoustic signal at source depth y_0 meters.
- $\beta(y_R)$ angle of arrival of incident plane wave field at depth y_R meters.
- β_{LOS} the line-of-sight angle, as measured from the positive Y axis, between the transmitter and the receive array.

Note that in Figure 2.1 the positive Y axis is defined in the direction of increasing depth, or in the downward direction. The coordinate system shown in Figure 2.1 is applicable for any relative positioning of the transmitter and receive array, even if ΔX , ΔY , and/or ΔZ are negative. Thus, the algorithm will work for any direction of arrival of the incident acoustic plane-wave field.

The receive array is assumed to possess knowledge of its own depth. In addition, the receive array will have available estimates of arrival direction cosines associated with the local angles of arrival. These estimates are computed by the frequency domain adaptive beamforming algorithm. From these known quantities and information about the local sound-speed profile, the transmitter's location with respect to the receiver shall be determined.

B. TRANSMITTER LOCALIZATION THEORY

Energy, whether it is acoustic or electromagnetic, will refract as it passes from a medium with index of refraction n_1 into a medium with index of refraction n_2 , provided that $n_1 \neq n_2$. In this study, the ocean volume is characterized by a one-dimensional index of refraction (sound-speed profile) that is a function of depth. Snell's law is given by [Ref. 1: p. 218],

$$\frac{\sin \beta(y)}{c(y)} = \frac{\sin \beta(y_0)}{c(y_0)} \quad (2.1)$$

where $c(y)$ is the speed of sound in meters per second at a depth y . From Snell's law a ray parameter may be defined as

$$b = \frac{\sin \beta(y_0)}{c(y_0)} = \frac{\sin \beta(y_R)}{c(y_R)} = \frac{\sin \beta(y_{TP})}{c(y_{TP})} = \frac{1}{c(y_{TP})} \quad (2.2)$$

where:

- b is the ray parameter.
- y_{TP} is the depth of a turning point. A turning point is defined as the point along a ray path at which the angle of propagation, $\beta(y_{TP})$, is equal to 90 degrees.

At this point $\beta(y_R)$ is known, since the direction cosine

$$v(y_R) = \cos \beta(y_R) \quad (2.3)$$

is calculated by the frequency domain adaptive beamforming algorithm. The speed of sound at depth y_R , denoted $c(y_R)$, is normally known aboard ship as a result of measurements made by onboard sonar systems.

It is assumed that the sound-speed profile is a linear function of depth with constant gradient. In most areas of the ocean this is a good approximation if both the transmitter and the receive array are in the same portion of the sound-speed profile. A typical sound-speed profile is shown in Figure 2.2. The parameter g is the constant gradient of the sound-speed profile in seconds⁻¹. From the surface to about 100 meters a positive gradient is typically observed with a gradient $g \approx +0.016 \text{ sec}^{-1}$ [Ref. 4: p. 30], [Ref. 5: p. 401]. Below 100 meters a negative gradient is present, and in this example $g \approx -0.02956 \text{ sec}^{-1}$. Finally, at depths between 700 to 1500 meters [Ref. 4: p. 32] the gradient reverts to a positive value of $g \approx +0.017 \text{ sec}^{-1}$ [Ref. 5: p. 401]. The value of g in the negative portion of the gradient was computed by assuming the speed of sound to be 1500 meters per second at the ocean surface and 1475 meters per second at a depth of 1000 meters [Ref. 6: p. 3]. A depth of 1000 meters was chosen as the starting point of the second positive gradient. The negative gradient was then calculated to fit between the positive gradients. Based on the assumption that both the transmitter and the receive array are in the same gradient of the sound-speed profile, the speed of sound at depth y can be found from

$$c(y) = c(y_0) + g(y - y_0) \quad (2.4)$$

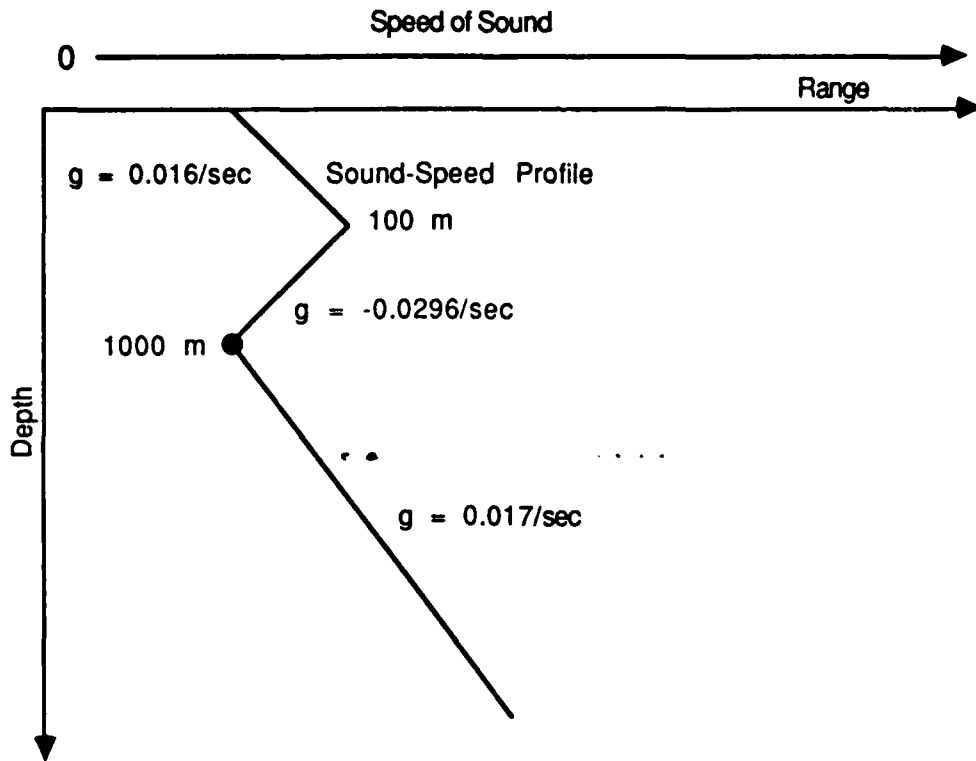


Figure 2.2 Typical Sound-Speed Profile.

The radius of curvature that describes the arc of the circle followed by an acoustic field propagating through this medium is then [Ref. 1: p. 237]

$$R_c = \frac{c(y_0)}{|g \sin \beta(y_0)|} = \frac{c(y_R)}{|g \sin \beta(y_R)|} \quad (2.5)$$

All the terms on the far righthand side of Equation 2.5 are known. Equation 2.4 may be rewritten as expressed by Ziomek [Ref. 1: p. 238]

$$y = y_0 + \frac{c(y) - c(y_0)}{g} \quad (2.6)$$

Therefore,

$$\Delta Y = y_R - y_0 = \frac{1}{g} c(y_R) - \frac{1}{g} c(y_0) \quad (2.7)$$

and, from equations 2.1 and 2.2,

$$c(y_R) = \frac{\sin \beta(y_R)}{b} \quad (2.8)$$

and

$$c(y_0) = \frac{\sin \beta(y_0)}{b} \quad (2.9)$$

Combining equations 2.8 and 2.9 with equation 2.7 it is readily observed that,

$$\Delta Y = y_R - y_0 = \frac{1}{bg} \sin \beta(y_R) - \frac{1}{bg} \sin \beta(y_0) \quad (2.10)$$

or,

$$\Delta Y = y_R - y_0 = a \sin \beta(y_R) - a \sin \beta(y_0) \quad (2.11)$$

where

$$a = \frac{1}{bg} \quad (2.12)$$

The only unknowns now in equation 2.11 are $\beta(y_0)$ and ΔY . Also note that

$$R_c = |a| = \text{radius of curvature.} \quad (2.13)$$

The radial distance ΔR shown in Figure 2.1 can be found by utilizing the following equation [Ref. 1: p. 238]:

$$z = z_0 + \frac{c(y_0)}{g \sin \beta(y_0)} [\cos \beta(y_0) - \cos \beta(y)] \quad (2.14)$$

which is the Z coordinate of a ray propagating in the YZ plane. In this thesis a more general class of problem is assumed so that the coordinate axes can remain fixed relative to the platform on which the planar array is mounted. Therefore, in a three-dimensional system, z and z₀ are replaced by the polar coordinates r and r₀ to give

$$r = r_0 + \frac{c(y_0)}{g \sin \beta(y_0)} [\cos \beta(y_0) - \cos \beta(y)] , \quad (2.15)$$

and, as a result,

$$\Delta R = r_R - r_0 = \frac{1}{bg} [\cos \beta(y_0) - \cos \beta(y_R)] \quad (2.16)$$

or

$$\Delta R = r_R - r_0 = a \cos \beta(y_0) - a \cos \beta(y_R) . \quad (2.17)$$

The only unknowns in equation 2.17 are $\beta(y_0)$ and ΔR . Also, note in Figure 2.1 that if

$$\Delta X = 0, \quad (2.18)$$

then

$$\Delta R = \Delta Z . \quad (2.19)$$

At this point ray acoustics cannot provide any further information to develop a solution to the problem. However, a model-based phase weight for a planar sonar array, similar to that shown in Figure 2.3 , can be used to localize the transmitter. As derived by Ziomek and Blount [Ref. 3]

$$\Phi_n(f) = -2\pi f \gamma_n d_Y + \Phi_{MD}(f,n) \quad n = -(N-1), 2, \dots, 0, \dots, (N-1) \quad (2.20)$$

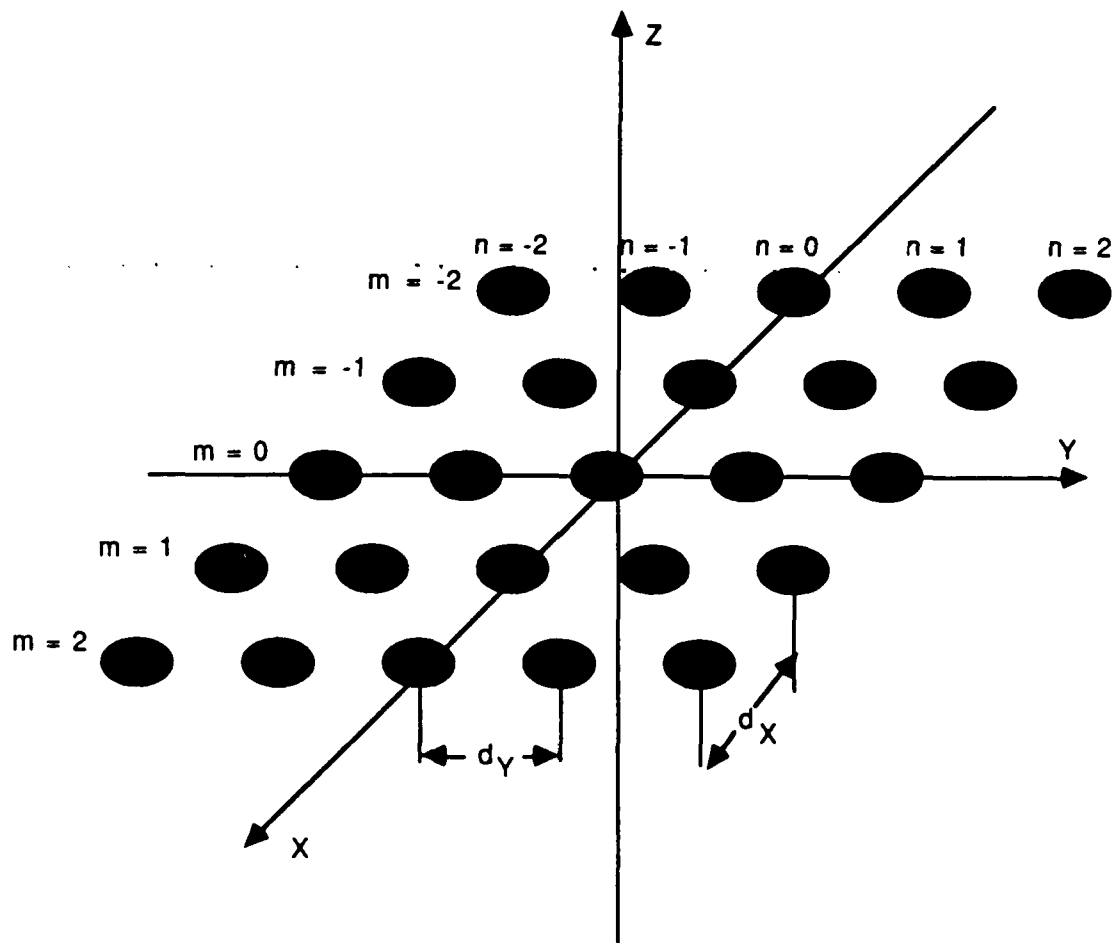


Figure 2.3 Receive Planar Array Geometry.

where

$$f_Y = \frac{-v_B f}{c(y_R)}, \quad (2.21)$$

$$v_B = \cos \beta(y_T), \quad (2.22)$$

and:

- $\Phi_n(f)$ is the phase weight in the Y direction associated with element (m,n) in the receive array.
- f is the frequency of the transmitted electrical signal.
- $\Phi_{MD}(f,n)$ is the model-based phase weight which is related to the deterministic angle modulation performed by the ocean medium on the transmitted electrical signal as a function of depth [Ref. 3].
- y_T is the depth of the transmit array.
- d_Y is the interelement spacing in the Y direction associated with the receive array.

Equation 2.20 describes the phase weights in the Y direction that a planar sonar array using the three-dimensional FFT beamformer presented by Ziomek and Blount [Ref. 3] would use to receive an acoustic signal transmitted from a depth y_T and received at a depth y_R . This equation can be seen to consist of two parts. The first portion is the term $-2\pi f_Y n d_Y$ which is the phase weight used in traditional beam steering. The second part, $\Phi_{MD}(f,n)$, is further described by Ziomek and Blount [Ref. 3] as

$$\Phi_{MD}(f,n) = -[k(y_T)/2v_B]\{[c(y_T)g][n'D(y_R + nd_Y) - 1] + \Delta Y_n\} \quad (2.23)$$

where the wave number in radians per meter as a function of depth y_T is

$$k(y_T) = 2\pi f c(y_T), \quad (2.24)$$

$$f = f_c + kf_0, \quad k = -K, \dots, 0, \dots, K. \quad (2.25)$$

$$n'_D(y_R + nd_Y) = \frac{c(y_T)}{c(y_T) + g\Delta Y_n}, \quad (2.26)$$

and,

$$\Delta Y_n = y_R - y_T + nd_Y, \quad (2.27)$$

where:

- f_c is the carrier frequency in hertz,
- f_0 is the fundamental frequency in hertz of the finite Fourier series representation of the complex envelope of the transmitted electrical signal, and
- K is the highest harmonic used in the finite Fourier series.

The term n'_D defines an index of refraction which is corrected for the distance that the (m,n) element in the receive array is offset in the Y direction from the center of the array. This compensation is provided by ΔY_n , which computes the depth separation between the center of the transmit array and the element (m,n).

When using these model-based phase weights it should be noted that y_T is equivalent to y_0 of Figure 2.1. Additionally,

$$v_B = \cos \beta(y_T) = \cos \beta(y_0). \quad (2.28)$$

Dividing equation 2.24 by $2v_B$ yields

$$\frac{k(y_T)}{2v_B} = \frac{2\pi f}{c(y_T)} \frac{1}{2v_B} = \frac{\pi f}{c(y_T)v_B}. \quad (2.29)$$

The term $n'_D(y_R + nd_Y) - 1$ may also be rewritten as

$$n'_D(y_R + nd_Y) - 1 = \frac{c(y_T)}{c(y_T) + g\Delta Y_n} - 1 \quad (2.30)$$

and, as a result,

$$n'_D(y_R + nd_Y) - 1 = \frac{c(y_T) - c(y_T) - g\Delta Y_n}{c(y_T) + g\Delta Y_n} \quad (2.31)$$

$$n'_D(y_R + nd_Y) - 1 = \frac{-g\Delta Y_n}{c(y_T) + g\Delta Y_n} \quad (2.32)$$

Therefore, substituting equations 2.32 and 2.29 into equation 2.23 yields

$$\Phi_{MD}(f,n) = \frac{-\pi f}{c(y_T)v_B} \frac{[-c(y_T)\Delta Y_n + c(y_T)\Delta Y_n + g\Delta Y_n^2]}{[c(y_T) + g\Delta Y_n]} \quad (2.33)$$

$$\Phi_{MD}(f,n) = \frac{-\pi f}{c(y_T)v_B} \frac{g\Delta Y_n^2}{[c(y_T) + g\Delta Y_n]} \quad (2.34)$$

Expanding the denominator of the second term on the right side of equation 2.34 results in

$$c(y_T) + g\Delta Y_n = c(y_T) + g(y_R - y_T + nd_Y) \quad (2.35)$$

From equation 2.4 it can be seen that

$$c(y_T) + g(y_R - y_T + nd_Y) = c(y_R + nd_Y) \quad (2.36)$$

Therefore,

$$c(y_T) + g\Delta Y_n = c(y_R + nd_Y) \quad (2.37)$$

Substituting equation 2.37 and equation 2.22 into equation 2.34 gives

$$\Phi_{MD}(f,n) = \frac{-\pi fg\Delta Y_n^2}{c(y_T)c(y_R + nd_Y) \cos \beta(y_T)} \quad (2.38)$$

From equation 2.2, with $y_T = y_0$

$$c(y_T) = \frac{\sin \beta(y_T)}{b} \quad (2.39)$$

and, as a result,

$$\Phi_{MD}(f,n) = \frac{-\pi f b g \Delta Y_n^2}{c(y_R + n d_Y) \sin \beta(y_T) \cos \beta(y_T)} \quad (2.40)$$

From equation 2.12,

$$a = \frac{1}{b g} \quad (2.12)$$

or

$$\frac{1}{a} = b g \quad (2.41)$$

Using equation 2.41 in equation 2.40 yields

$$\Phi_{MD}(f,n) = \frac{-\pi f \Delta Y_n^2}{a c(y_R + n d_Y) \sin \beta(y_T) \cos \beta(y_T)} \quad (2.42)$$

where

$$\Delta Y_n = y_R - y_T + n d_Y = \Delta Y + n d_Y \quad (2.43)$$

If the center element of the receive array is chosen as the element at which the phase weight $\Phi_{MD}(f,n)$ is calculated, then $n = 0$, and

$$\Delta Y_0 = \Delta Y = y_R - y_T \quad (2.44)$$

Therefore, at $n = 0$

$$\Phi_{MD}(f,0) = \frac{-\pi f \Delta Y^2}{ac(y_R) \sin \beta(y_T) \cos \beta(y_T)} \quad (2.45)$$

Now squaring both sides of equation 2.10 will result in

$$\Delta Y^2 = a^2 \sin^2 \beta(y_0) - 2a^2 \sin \beta(y_R) \sin \beta(y_0) + a^2 \sin^2 \beta(y_R) \quad (2.46)$$

which can be used in equation 2.45 to replace ΔY^2 . Now let

$$x = \sin \beta(y_0) \quad (2.47)$$

and

$$y = \cos \beta(y_0) \quad (2.48)$$

The x and y defined in equations 2.47 and 2.48 are not the x and y coordinates related to Figure 2.1. Rather, this x and y are merely dummy variables to be used in the solution of equation 2.45. Due to the definitions of equations 2.47 and 2.48 a relationship between the variables x and y is apparent, that is,

$$x^2 + y^2 = 1 \quad (2.49)$$

and, therefore,

$$y = \pm (1 - x^2)^{1/2} \quad (2.50)$$

Next, replace y_T with y_0 in equation 2.45, substitute equation 2.46 into equation 2.45, and multiply equation 2.45 by $ac(y_R)xy$. This results in

$$ac(y_R)\Phi_{MD}(f,0)xy = -\pi f [a^2x^2 - 2a^2 \sin \beta(y_R)x + a^2 \sin^2 \beta(y_R)] \quad (2.51)$$

Divide both sides of equation 2.51 by πfa^2 to get

$$\frac{c(y_R)}{\pi f a} \Phi_{MD(f,0)xy} = -x^2 + 2 \sin \beta(y_R)x - \sin^2 \beta(y_R). \quad (2.52)$$

Rewriting equation 2.52 yields

$$x^2 + \frac{c(y_R)}{\pi f a} \Phi_{MD(f,0)xy} - 2 \sin \beta(y_R)x + \sin^2 \beta(y_R) = 0 \quad (2.53)$$

or

$$Ax^2 + Bxy + Cx + D = 0 \quad (2.54)$$

where

$$A = 1.0, \quad (2.55)$$

$$B = \frac{c(y_R)}{\pi f a} \Phi_{MD(f,0)}, \quad (2.56)$$

$$C = -2 \sin \beta(y_R), \quad (2.57)$$

and

$$D = \sin^2 \beta(y_R). \quad (2.58)$$

Substituting equation 2.50 into equation 2.54 yields

$$Ax^2 \pm Bx(1-x^2)^{1/2} + Cx + D = 0 \quad (2.59)$$

or,

$$Ax^2 + Cx + D = \pm Bx(1-x^2)^{1/2}. \quad (2.60)$$

Squaring both sides of equation 2.60 gives

$$(Ax^2 + Cx + D)^2 = B^2x^2(1 - x^2) = B^2x^2 - B^4x^4. \quad (2.61)$$

Expanding equation 2.61 yields

$$A^2x^4 + 2ACx^3 + (2AD + C^2)x^2 + 2CDx + D^2 = B^2x^2 - B^4x^4 \quad (2.62)$$

or

$$(A^2 + B^2)x^4 + 2ACx^3 + (2AD - B^2 + C^2)x^2 + 2CDx + D^2 = 0. \quad (2.63)$$

To find the unknown, x , the roots of equation 2.63 must be computed. These roots will also be the roots of equation 2.59. In the computer algorithm written to implement this theory, the value

$$F(x,y) = Ax^2 \pm Bx(1 - x^2)^{1/2} + Cx + D \quad (2.64)$$

was also calculated to verify the validity of the roots found for equation 2.63.

Recalling that equation 2.47 defined

$$x = \sin \beta(y_0) \quad (2.47)$$

and equation 2.48 defined

$$y = \cos \beta(y_0), \quad (2.48)$$

we see that once x and y are known they may be substituted into equations 2.11 and 2.17 to solve for ΔY and ΔR (since $\beta(y_R)$, the radius of curvature (a), the receive array depth, and the local sound-speed profile are all known).

At this point ΔY , ΔR and $\beta(y_0)$ are known. The next values to be found are ΔX , ΔZ , RLOS, and β LLOS. Using the definitions of the direction cosines as presented by Ziomek [Ref. 1: p.226]

$$v = \cos \beta(y), \quad (2.65)$$

$$u = \cos \alpha(y), \quad (2.66)$$

and

$$w = \cos \gamma(y) \quad (2.67)$$

where:

- $\alpha(y)$ is the angle at a depth y measured from the positive X axis to the vector of interest.
- $\gamma(y)$ is the angle at a depth y measured from the positive Z axis to the vector of interest.

Referring to Figure 2.1, the direction cosine $v(y)$ at the transmitter depth can be written as

$$v(y_0) = \cos \beta(y_0) = \frac{\Delta Y}{\text{HRLOS}} \quad (2.68)$$

and, as a result,

$$\text{HRLOS} = \frac{\Delta Y}{v(y_0)}. \quad (2.69)$$

Also from Figure 2.1 it can be observed that

$$\text{HRLOS}^2 = \text{HDLTR}^2 + \Delta Y^2. \quad (2.70)$$

In ray acoustics, as presented by Ziomek [Ref. 1: p.223], the propagation vector is defined as

$$\mathbf{k} = k_X \mathbf{x} + k_Y \mathbf{y} + k_Z \mathbf{z} \quad (2.71)$$

where

$$k_X = k_0 u, \quad (2.72)$$

$$k_Y = k_0 v, \quad (2.73)$$

$$k_Z = k_0 w, \quad (2.74)$$

and

$$k_0 = \frac{2\pi f}{c(y_0)}. \quad (2.75)$$

Therefore, at the transmitter,

$$k_{XT} = \frac{2\pi f}{c(y_T)} u(y_T), \quad (2.76)$$

and, at the receive array,

$$k_{XR} = \frac{2\pi f}{c(y_R)} u(y_R). \quad (2.77)$$

Additionally, for an inhomogeneous medium which has a sound-speed profile that is a function of depth only, it is known that [Ref. 1: p.223]

$$k_{XR} = k_{XT} = \text{constant}. \quad (2.78)$$

Therefore, from equations 2.76 and 2.77,

$$\frac{2\pi f}{c(y_R)} u(y_R) = \frac{2\pi f}{c(y_T)} u(y_T) \quad (2.79)$$

so that

$$u(y_R) = \frac{c(y_R)}{c(y_T)} u(y_T) \quad (2.80)$$

or,

$$u(y_T) = \frac{c(y_T)}{c(y_R)} u(y_R). \quad (2.81)$$

In equation 2.81 $u(y_R)$ is supplied by the beamformer, $c(y_R)$ is known by own ship, and since equation 2.11 has been solved for ΔY , it is possible to use equation 2.4 to calculate $c(y_T)$. Therefore, $u(y_T)$ becomes a known quantity. An alternate method of determining $c(y_T)$ would be by the use of Snell's law, or equation 2.1, since $\beta(y_R)$, $\beta(y_T)$ and $c(y_R)$ are all known.

Similarly [Ref. 1: p. 233],

$$k_{ZR} = k_{ZT} \quad (2.82)$$

and, as a result,

$$w(y_T) = \frac{c(y_T)}{c(y_R)} w(y_R). \quad (2.83)$$

Referring to Figure 2.1 and utilizing equation 2.81 it can be seen that

$$u(y_0) = \cos \alpha(y_0) = \frac{c(y_0)}{c(y_R)} u(y_R) = \frac{HDLTX}{HRLOS}. \quad (2.84)$$

Therefore, since $u(y_0)$ is known from substituting y_0 for y_T in equation 2.81, the value of HDLTX is given by

$$HDLTX = u(y_0)HRLOS. \quad (2.85)$$

Now that $u(y_0)$ and $v(y_0)$ are known from equation 2.84 and equation 2.68, it is possible to find $w(y_0)$ by use of the fact that [Ref. 1: p. 224]

$$w^2(y_0) = 1 - u^2(y_0) - v^2(y_0). \quad (2.86)$$

Again utilizing Figure 2.1 and the fact that

$$w(y_0) = \cos \gamma(y_0), \quad (2.87)$$

we see that

$$w(y_0) = \frac{HDLTZ}{HRLOS}. \quad (2.88)$$

Therefore,

$$HDLTZ = w(y_0) HRLOS. \quad (2.89)$$

Figure 2.4 shows the geometry of Figure 2.1 as seen by looking down into the XZ plane from above the transmitter's depth. From Figure 2.4 the relationships between ΔZ , ΔX , and ΔR may be derived.

The angle δ in Figure 2.4 can be found from

$$\tan \delta = \frac{HDLTX}{HDLTZ}. \quad (2.90)$$

Therefore,

$$\delta = \tan^{-1}(HDLTX, HDLTZ). \quad (2.91)$$

Substituting equations 2.85 and 2.89 into equation 2.91 results in

$$\delta = \tan^{-1}\{[u(y_0)HRLOS] \cdot [w(y_0)HRLOS]\} \quad (2.92)$$

so that

$$\delta = \tan^{-1}[u(y_0) w(y_0)]. \quad (2.93)$$

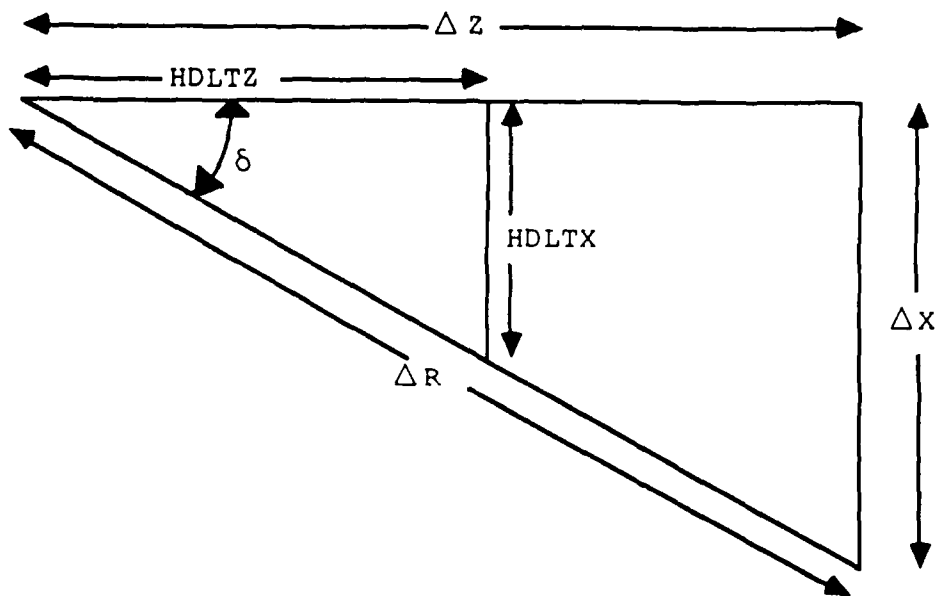


Figure 2.4 Topview of Geometry.

For an inhomogeneous medium with a sound-speed profile that is a function of depth only, it can be shown that [Ref. 1: p. 232]

$$\frac{u(y)}{w(y)} = \text{constant} . \quad (2.94)$$

Therefore,

$$\delta = \tan^{-1}[u(y_R) \cdot w(y_R)] \quad (2.95)$$

where $u(y_R)$ and $w(y_R)$ are available from the frequency domain adaptive beamformer. From Figure 2.4, ΔZ and ΔX are given by

$$\Delta Z = \Delta R \cos \delta \quad (2.96)$$

and

$$\Delta X = \Delta R \cos \delta . \quad (2.97)$$

Referring once again to Figure 2.1, RLOS is given by

$$RLOS = (\Delta X^2 + \Delta Y^2 + \Delta Z^2)^{1/2} \quad (2.98)$$

or, since

$$\Delta R^2 = \Delta X^2 + \Delta Z^2 , \quad (2.99)$$

$$RLOS = (\Delta R^2 + \Delta Y^2)^{1/2} . \quad (2.100)$$

Finally, β_{LOS} can be determined by using

$$\beta_{LOS} = \cos^{-1}(\Delta Y/RLOS) . \quad (2.101)$$

The equations presented in this section comprise the theory used to develop the model-based localization algorithm. By the use of ray acoustics and the assumption that the model-based phase weight is known, a closed form solution is possible for the localization problem. Obviously, the solution's accuracy depends on a ship's ability to correctly measure the sound-speed profile and the effects of any other local sonar conditions, such as shallow depths and the presence of biologics. However, in the open ocean, when the transmitter and receiver are located in the same gradient of the sound-speed profile, a reasonably accurate solution is possible. There are some limitations involved with the use of ray acoustics and the model-based phase weights. These limitations will be discussed in the next section.

C. LIMITATIONS OF RAY ACOUSTICS SOLUTION

1. Turning Points

A turning point is that position along a ray path propagating through an inhomogeneous medium at which the angle of propagation measured with respect to the positive Y axis, $\beta(y)$, is equal to 90 degrees. At this point the origination of the ray path becomes ambiguous to a receiver using the localization technique described in this

thesis, because there is no way of knowing how many turning points the acoustic signal has passed through. The turning point will cause a transmitter that is below (above) the receiver to appear to be above (below) the receiver. Figure 2.5 illustrates these two possibilities. In the case of receiver one in Figure 2.5, a turning point has occurred between the transmitter's location and the receiver's location. The theory presented in this section would result in a calculated line-of-sight similar to that shown in Figure 2.5. The acoustic signal passes through two turning points prior to reaching receiver two, and the resulting line-of-sight calculation would indicate that the transmitter is at a depth below receiver two.

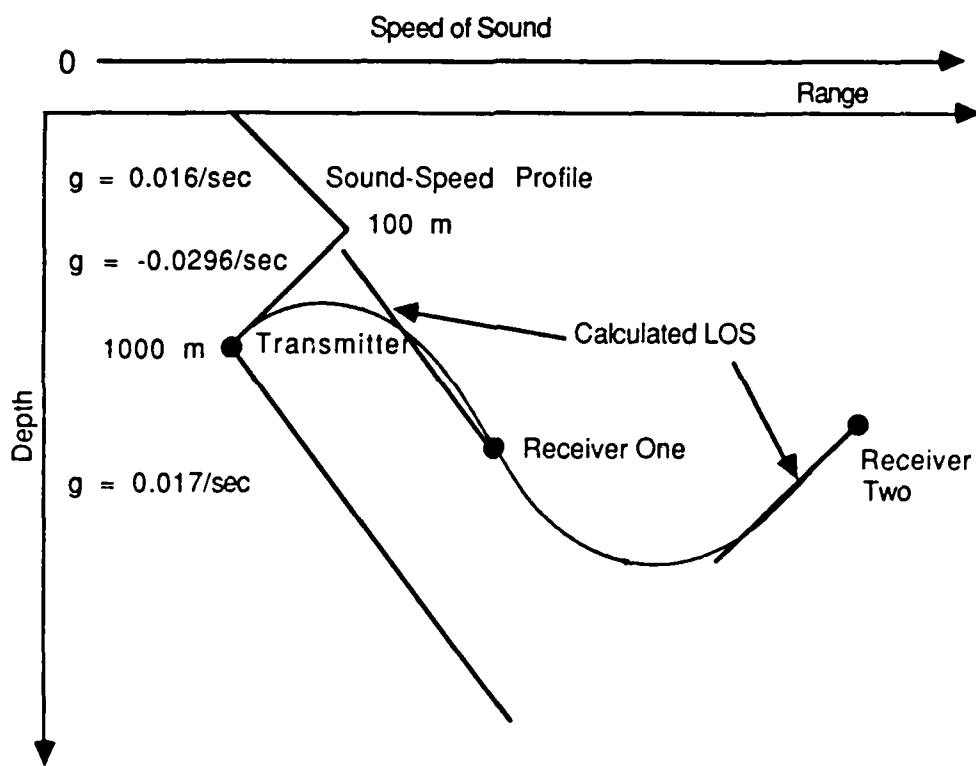


Figure 2.5 Turning Point Ambiguity.

The turning point ambiguity problem is not necessarily very restrictive, depending on local sonar conditions. Table 1 lists the location of turning points in terms of ΔY and ΔR between the transmitter and receive array. The values in Table 1 were calculated by assuming the values for $\beta(y_0)$, $c(y_0)$, and g shown in Table 1, and

then using equations 2.11 and 2.17 with $\beta(y_R) = 90^\circ$. These results show that for most angles of transmission the floor of the ocean would be reached prior to the signal reaching a turning point. Even at angles of transmission greater than 60 degrees the ranges to a turning point are quite large.

TABLE 1
DEPTH AND RANGE TO TURNING POINTS FOR A POSITIVE
GRADIENT

$\beta(y_0)$	ΔY (km)	ΔR (km)
10°	412.913	492.043
20°	166.935	238.343
30°	86.765	150.276
40°	48.241	103.424
50°	35.921	86.765
60°	13.449	50.063
70°	5.570	31.582
80°	1.336	15.271
85°	0.331	7.592

$$c(y_0) = 1475 \text{ m/sec}$$

$$g = 0.017 \text{ sec}^{-1}$$

If the transmitter and receive array are located in the negative gradient portion of the sound-speed profile as shown in Figure 2.5, the situation becomes much more restrictive. Here the transmitter must transmit in the upward direction to reach a turning point, as opposed to the downward transmission assumed in Table 1. Table 2 contains the results of calculations for the turning points in this region. In this case, the angles were only varied from 91 degrees to 100.8 degrees in order to place the turning point within the negative portion of the sound-speed profile of Figure 2.5. Even with the higher magnitude gradient used in Table 2, ranges of several thousand meters are achievable prior to the turning point. Note that all distances in Table 2 are in meters, whereas those listed in Table 1 are in kilometers.

TABLE 2
DEPTH AND RANGE TO TURNING POINTS FOR A NEGATIVE
GRADIENT

$\beta(y_0)$	ΔY (m)	ΔR (m)
91.0°	-7.601	870.982
93.0°	-68.478	2615.070
95.0°	-190.604	4365.554
97.0°	-374.729	6126.767
99.0°	-621.991	7903.148
100.0°	-769.765	8798.454
100.2°	-801.279	8978.159
100.4°	-833.451	9158.091
100.6°	-866.283	9338.253
100.8°	-899.777	9518.650

$c(y_0) = 1475$ m. sec $g = -0.02956$ sec⁻¹

2. Changes in Sound-Speed Profile

The transmitter and receiver must be in the same gradient of the sound-speed profile for the theory presented in this thesis to work. If the transmitter and receiver were located in different gradients of the sound-speed profile, a false location would be indicated due to the change in local angle of arrival. This situation is illustrated in Figure 2.6.

3. Validity of Model-Based Phase Weights

The development of the model-based phase weights is based in part on the assumption presented by Ziomek [Ref. 1: p.253] that if

$$|[n^2(y) - 1] v^2(y_0)| \ll 1, \quad (2.102)$$

then

$$k_Y(y) \approx k_Y + k_0^2 [n^2(y) - 1] (2k_Y) \quad (2.103)$$

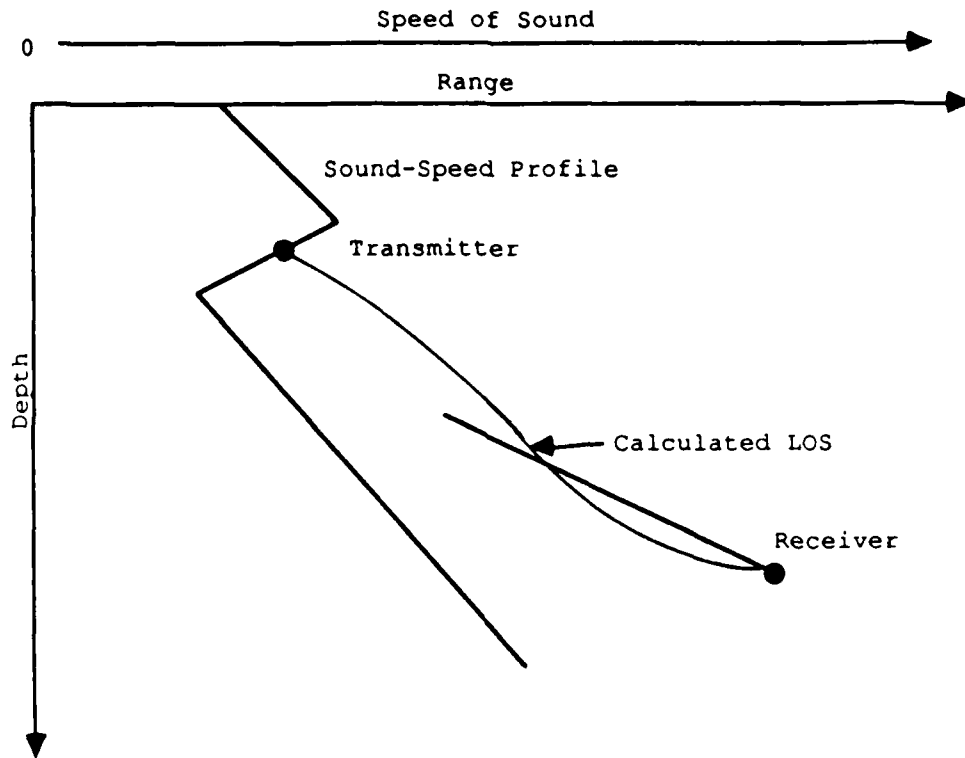


Figure 2.6 Changing Sound-Speed Gradient.

where

$$n(y) = \frac{c(y_0)}{c(y_R)} \quad (2.104)$$

and

$$k_Y = k(y_0)v(y_0) = \frac{2\pi f}{c(y_0)} v(y_0). \quad (2.105)$$

For some cases, such as $\beta(y_0)$ approaching 90 degrees, $v(y_0)$ becomes very small, resulting in the criteria of equation 2.102 being violated. In these instances the model-based phase weights can no longer be considered valid. Computations were performed prior to running the test cases presented in this thesis to ensure that test

cases which violate equation 2.102 were identified and not misrepresented as valid test cases.

In addition, the WKB approximation, which is the basis for the development of the model-based phase weights, becomes invalid as $k_Y(y)$ approaches zero [Ref. 1: p. 213]. This is the case at a turning point.

4. Depth Separation of Zero Meters

If $\Delta Y = 0.0$, meters the angle of transmission, $\beta(y_0)$, and the local angle of arrival, $\beta(y_R)$, must both be equal to 90 degrees to permit the receive array to receive any signal without that signal having to pass through a turning point. The algorithm fails here due to its invalidity at turning points and, as can be observed in equation 2.17, because ΔR would always be computed as zero. Obviously, a $\Delta Y = 0.0$ meters does not necessarily imply that $\Delta R = 0.0$ meters, since this condition is normally known as a collision.

III. COMPUTER IMPLEMENTATION OF LOCALIZATION THEORY

A. PROGRAM DESCRIPTION

The implementation of the theory described in Chapter II was performed by writing the FORTRAN computer program LOCATE. LOCATE is designed to operate as a subroutine in the frequency domain adaptive beamforming algorithm developed by Ziomek and Chan [Ref. 2]. LOCATE contains one subroutine, PLOTTER, which creates plots of the function described by equation 2.64. The description of LOCATE that follows demonstrates the relationship between the equations of Chapter II and the flow diagrams, however, the actual FORTRAN statements are not presented. After LOCATE is explained, there is a short discussion of PLOTTER. Section B discusses the method by which the algorithm was validated. Section C provides the actual results as compared to known geometries, and gives a comparison of double precision versus single precision results.

1. Program LOCATE

The program LOCATE uses as inputs the estimated direction cosines for local angles of arrival, model-based phase weights, and knowledge of the local sound-speed profile to determine ΔZ , cross-range (ΔX), depth separation (ΔY), and the line-of-sight range (RLOS) to the transmitter. Also, elevation depression angle and azimuthal angle to the transmitter are provided by LOCATE.

The elevation depression angle, as shown in Figure 3.1, is defined as the minimum angle between the receive planar sonar array's XZ plane and the line-of-sight between the transmitter and the receive array. The elevation depression angle is defined to be positive (elevation) if the transmitter's depth is less than the receiver's depth. If the transmitter is at a greater depth than the receive array the elevation depression angle is negative (depression). Therefore the elevation depression angle ranges in value from -90 degrees to +90 degrees.

The azimuthal angle, as shown in Figure 3.2, is defined as the minimum angle between the receive planar sonar array's Z axis and the line-of-sight between the transmitter and receive array, in the receive array's XZ plane. The azimuthal angle then ranges from +180 degrees to 0 degrees for positive ΔX and from 0 degrees to -180 degrees for negative ΔX .

The inputs to the program LOCATE are defined as follows:

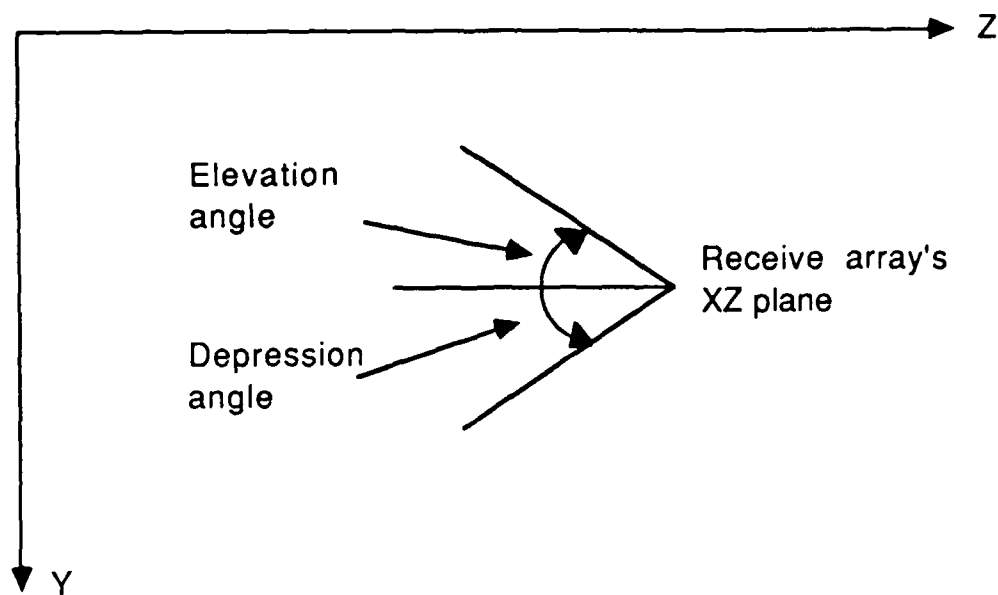


Figure 3.1 Elevation, Depression Angle.

- UYR, VYR, WYR estimates of direction cosines $u(y_R)$, $v(y_R)$, and $w(y_R)$, respectively, as calculated by the frequency domain adaptive beamformer.
- PIII model-based phase weights.
- FREQC carrier frequency of the received electrical signal.
- F0 fundamental frequency of the finite Fourier series representation of the complex envelope of the received electrical signal.
- G gradient of local sound-speed profile.
- CYR speed of sound at receive array depth y_R .
- NTOTAL total number of receive elements along the receive array's Y axis.
- QPRIME, QTOTAL parameters used to determine which harmonic is to be used in current calculations.
- NPRIME parameter used to determine which element's phase weight to use.

All the inputs are currently available from the frequency domain adaptive beamforming algorithm described by Ziomek and Chan [Ref. 2], with the exception of PIII. Figures 3.3 and 3.4 illustrates the flow of the program LOCATE.

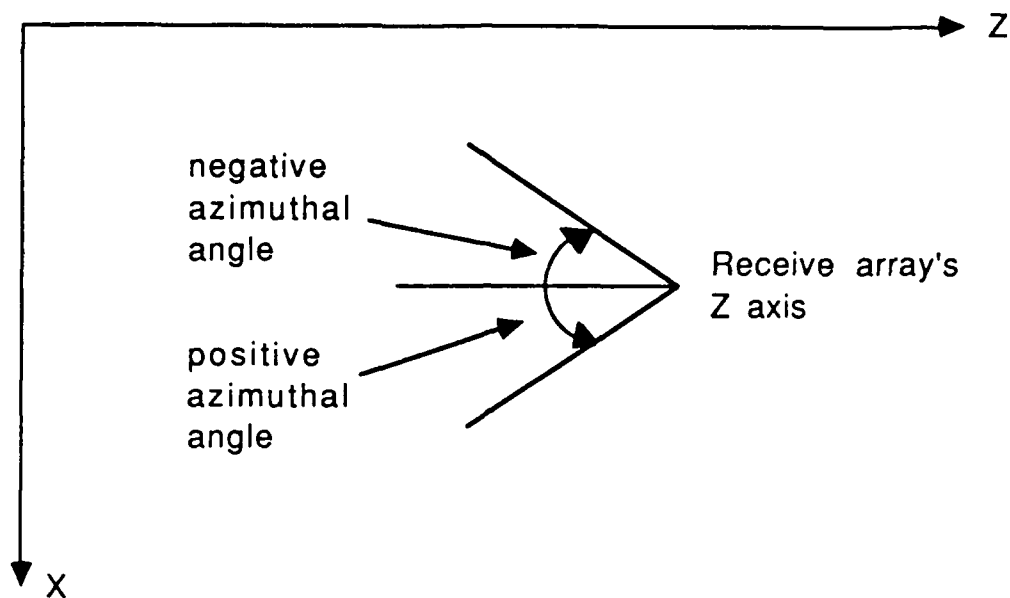


Figure 3.2 Azimuthal Angle.

The beamforming algorithm is written in single precision FORTRAN. However, the program LOCATE must operate in double precision to enable it to develop accurate roots for equation 2.63. Therefore, the values passed to LOCATE from the adaptive beamforming algorithm must be converted to double precision, either in LOCATE, or before they are sent to LOCATE. In this thesis, all values passed to LOCATE were double precision values. For testing purposes, only the portions of the adaptive beamforming program which develop values required by LOCATE were used, along with a program entitled SOUNDRAV, which generates the true problem geometry. The reasons for the use of double precision and the support programs used in testing LOCATE are further described in Section III.B.1.

Once the program LOCATE is entered, a loop parameter QTEMP = 1, QTOTAL is established. From QTEMP, an index Q for the harmonic of interest is chosen. This value Q is then used to determine the frequency F that will be used for further computations.

To calculate the ray parameter SMB the local angle of arrival, $\beta(y_R)$, is first found by the arc cosine of VYR. Then SMB is calculated by equation 2.2, using CYR

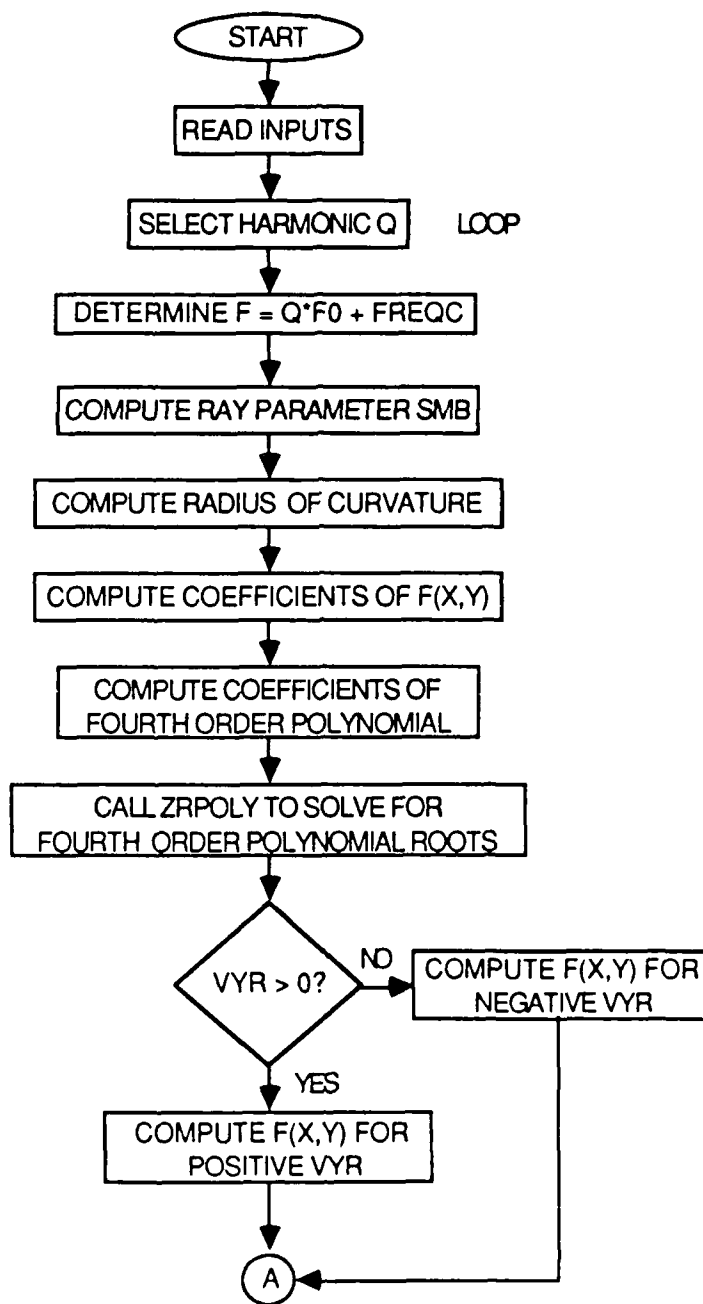


Figure 3.3 Program LOCATE Flowchart.

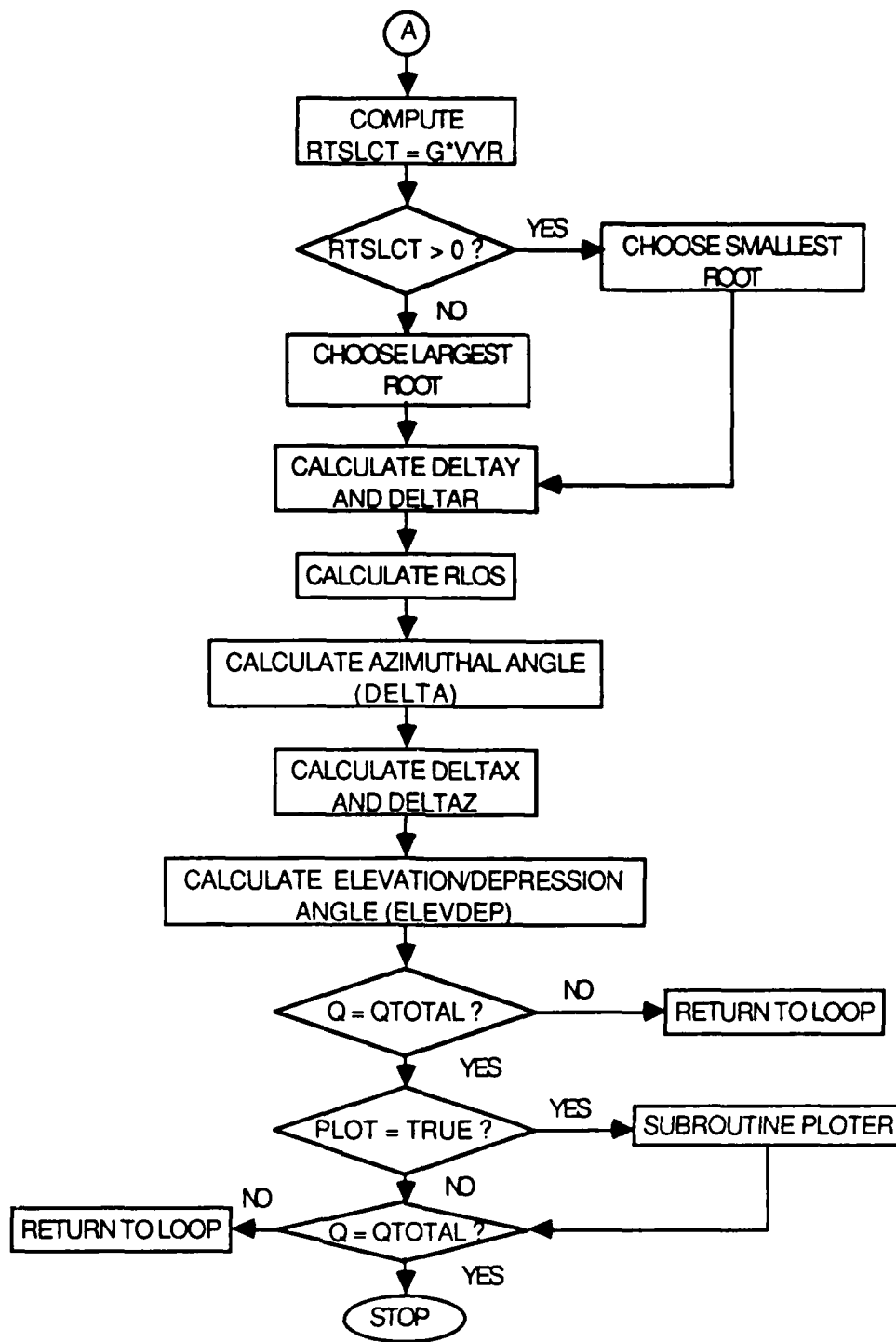


Figure 3.4 Program LOCATE Flowchart.

and $\beta(y_R)$. The value of G is passed to LOCATE by the adaptive beamformer, so SMA, the radius of curvature, is now found by using equation 2.12. At this point, equations 2.55 through 2.58 are utilized to determine the coefficients A, B, C, and D. These coefficients are in turn used to find the coefficients of equation 2.63, which are stored in an array called COEFF.

To determine the roots of equation 2.63, the double precision IMSL subroutine ZRPOLY is called, using the array COEFF as the input. ZRPOLY returns complex roots for equation 2.63 in an array called LAMBDA. In all the test cases that were run, the four roots in LAMBDA always consisted of two real roots and two complex roots. As a check of the validity of the roots, the value of $F(x,y)$ from equation 2.64 was calculated. A graph of the function $F(x,y)$, such as that shown in Figure 3.5, was used to determine whether to use $+(1 - x^2)^{1/2}$ or $-(1 - x^2)^{1/2}$ in this computation of $F(x,y)$.

The graphs indicated that for positive values of VYR the real roots are associated with the $+(1 - x^2)^{1/2}$ term, while the complex roots are associated with the $-(1 - x^2)^{1/2}$ term. This can be seen in Figure 3.5 where the curve associated with $-(1 - x^2)^{1/2}$ does not cross the $F(x,y) = 0$ line. The graph in Figure 3.5 only shows a small portion of the X axis. Test runs demonstrated that $F(x,y)$ increases as x varies from the x value corresponding to the minimum value of $F(x,y)$, in both the positive and negative X directions over the range $0 \leq x \leq 1$. Therefore, the graphs were expanded in the region close to the minimum of $F(x,y)$ to provide better resolution.

To continue with the calculations, one of the four roots must be selected as the value x of equation 2.47. No logic in the theory section, however, provides any basis for a decision as to which root is correct. The complex roots were disregarded because they cannot equate to x in equation 2.47. In order to determine a relationship which would allow programming logic to select the correct root from the two real roots found by ZRPOLY, numerous test cases with known transmitter and receive array locations were run using the four possible geometries allowed by the constraints listed on page six of this thesis. These geometries are:

1. transmitter above receive array, $0^\circ \leq \beta(y_0) < 90^\circ$, $G > 0$.
2. transmitter below receive array, $90^\circ < \beta(y_0) \leq 180^\circ$, $G > 0$.
3. transmitter above receive array, $0^\circ \leq \beta(y_0) < 90^\circ$, $G < 0$.
4. transmitter below receive array, $90^\circ < \beta(y_0) \leq 180^\circ$, $G < 0$.

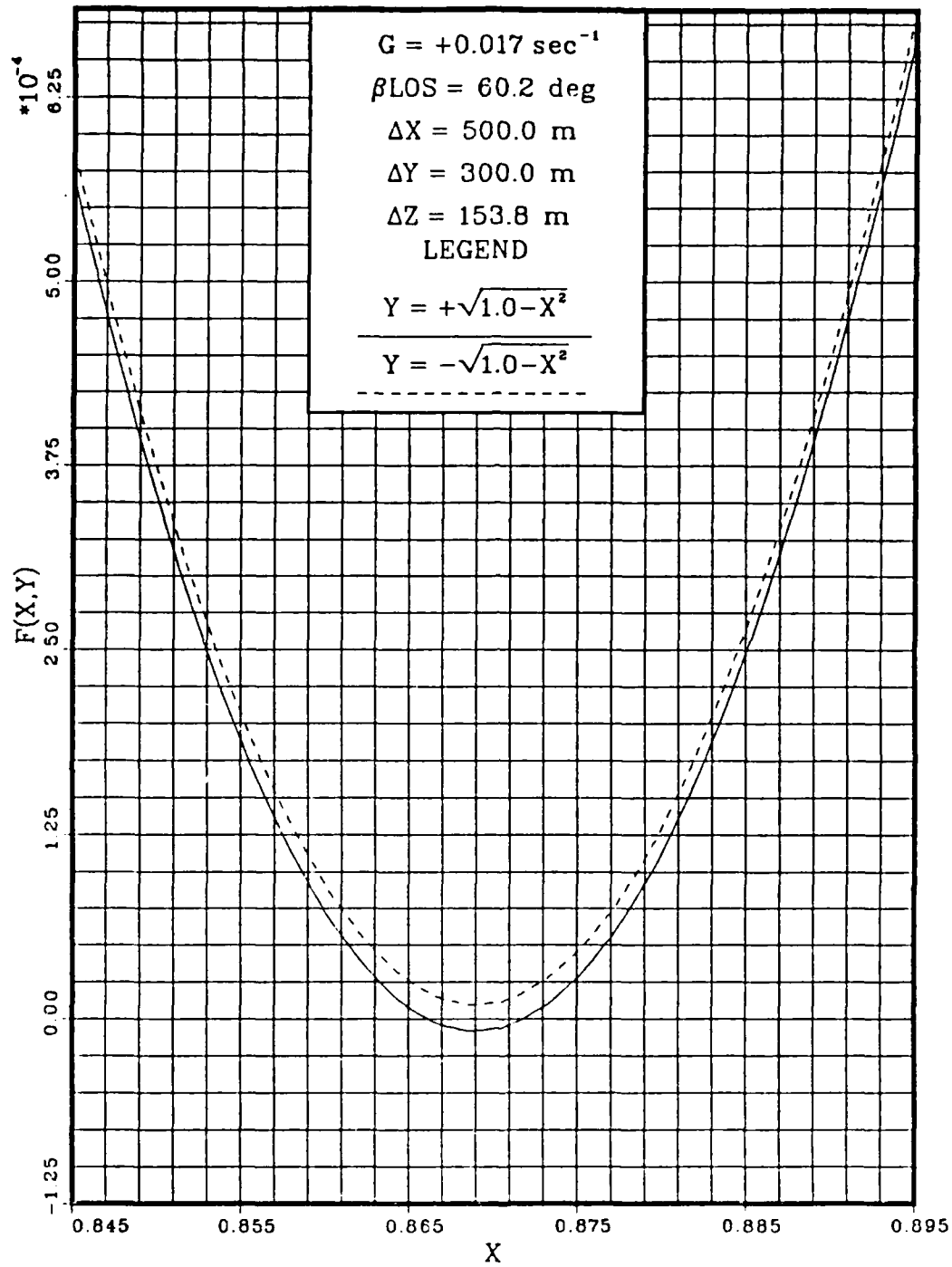


Figure 3.5 $F(x,y)$ for Geometry 1.

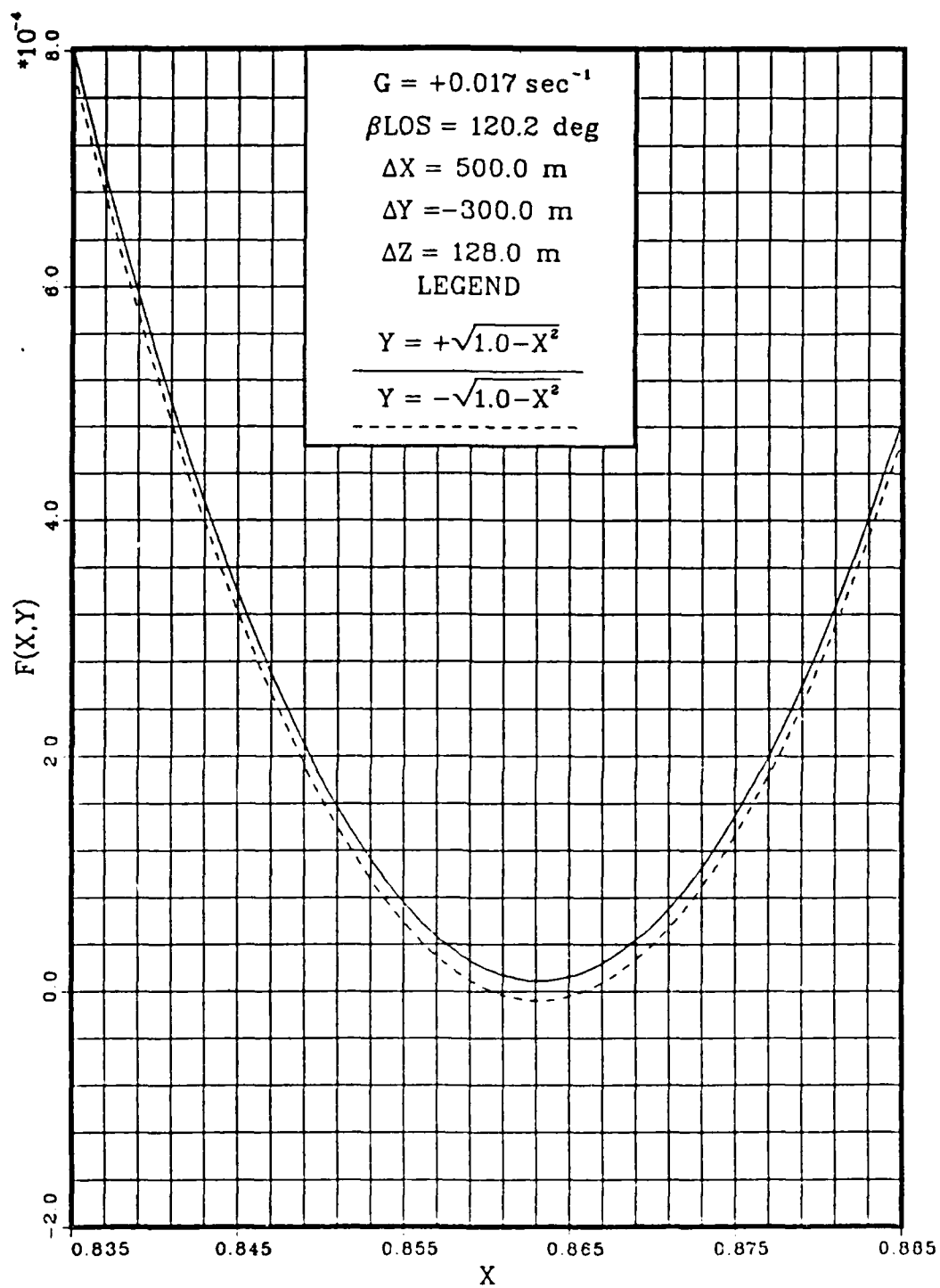


Figure 3.6 $F(x,y)$ for Geometry 2.

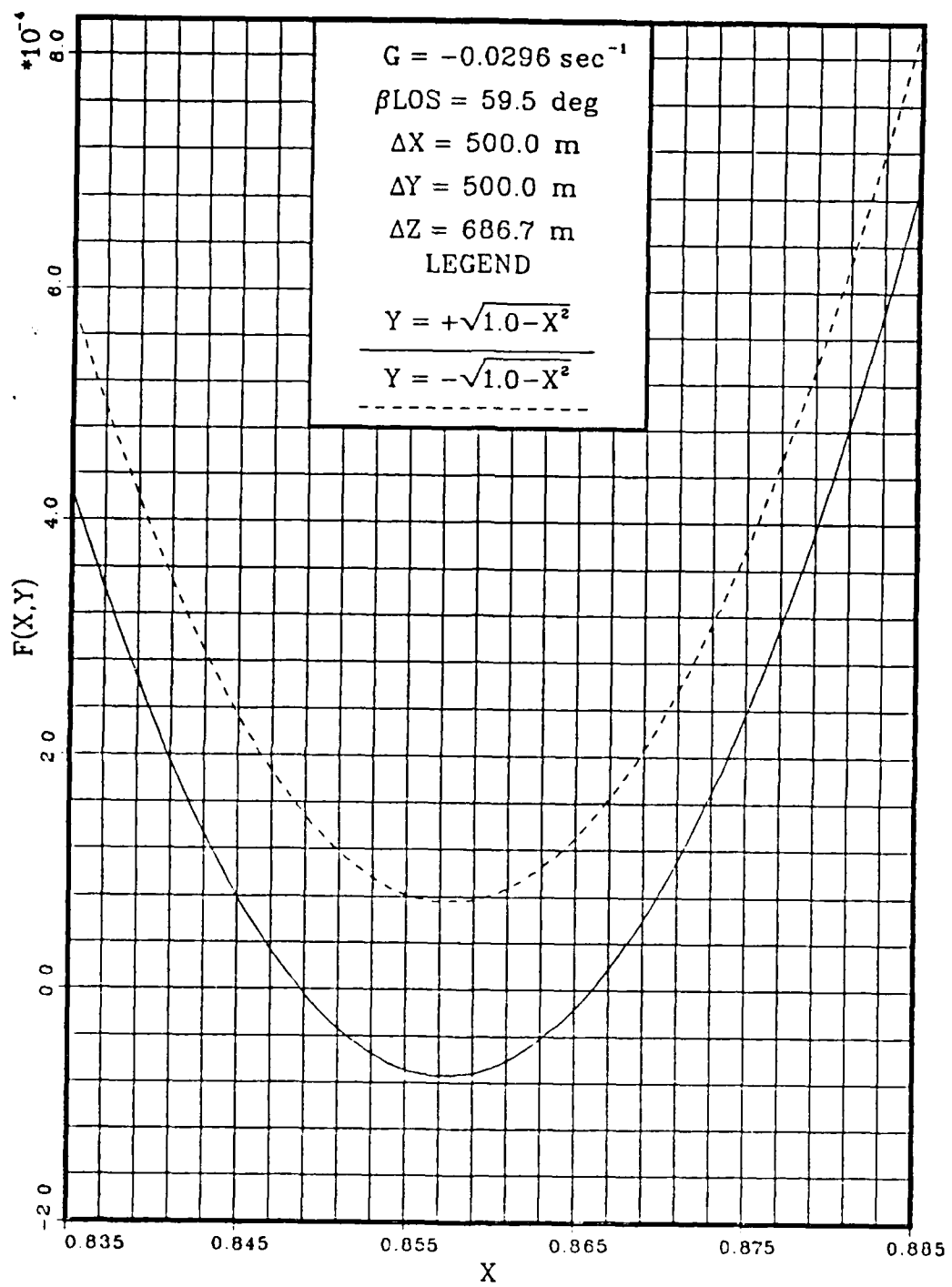


Figure 3.7 F(x,y) for Geometry 3.

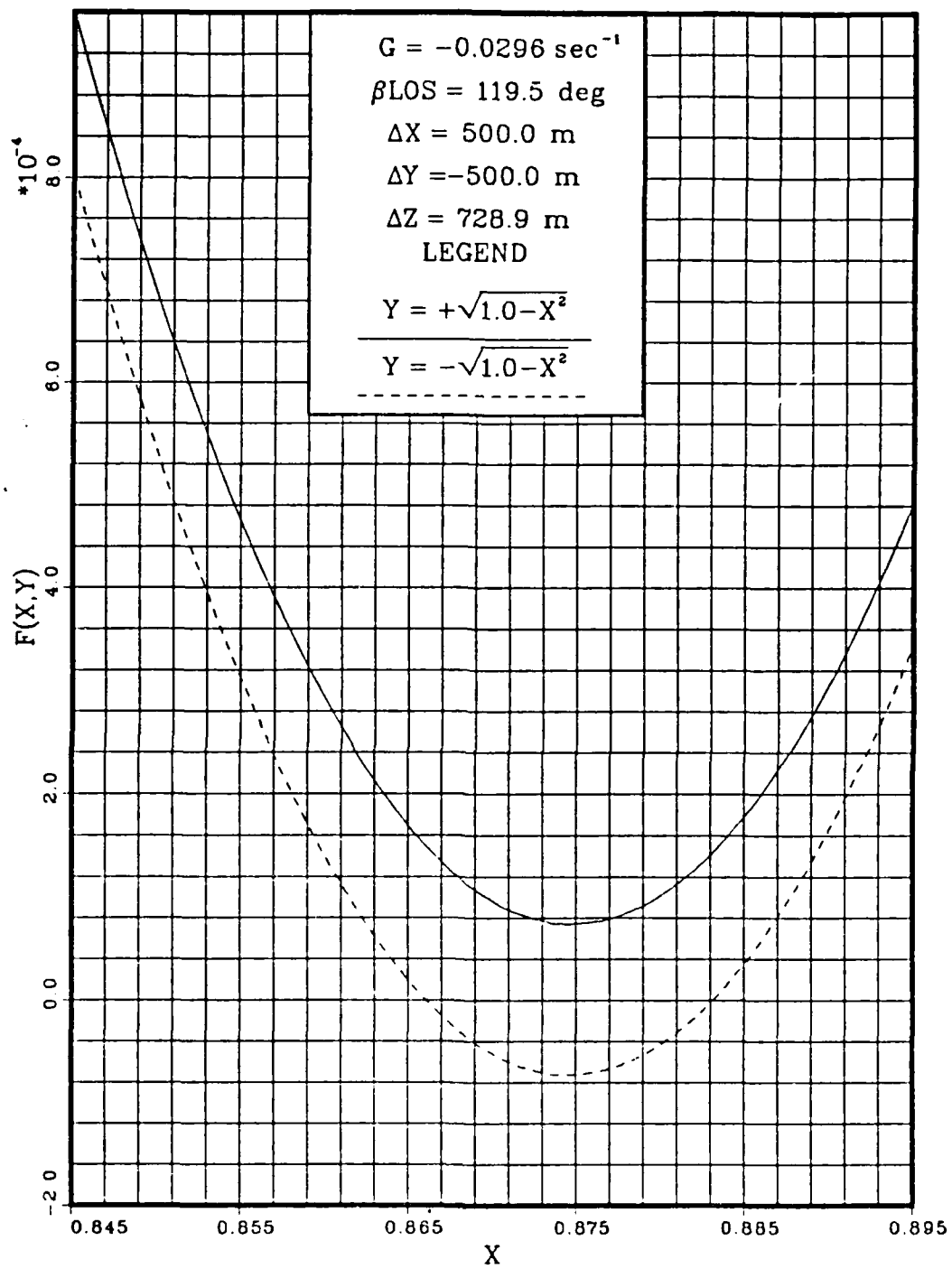


Figure 3.8 F(x,y) for Geometry 4.

- G gradient of the local sound-speed profile.
- DELTAX, DELTAY, DELTAZ cross-range, depth, and Z coordinate separations calculated by the program LOCATE.
- β LOS the line-of-sight angle as calculated by LOCATE.

The values of G , DELTAX, DELTAY, and DELTAZ are printed out on the graph as G , ΔX , ΔY , and ΔZ , respectively, to provide a means of identifying the geometry of the case corresponding to each graph.

The values A , B , C , D , and G are converted to single precision values prior to being passed from LOCATE to PLOTTER, because PLOTTER was written using DISSPLA which operates only in single precision. Due to the single precision accuracy of DISSPLA, plots made by PLOTTER are not accurate enough to determine the roots of equation 2.64. However the plots do show approximately where the roots occur. Figure 3.9 illustrates the flow of the subroutine PLOTTER.

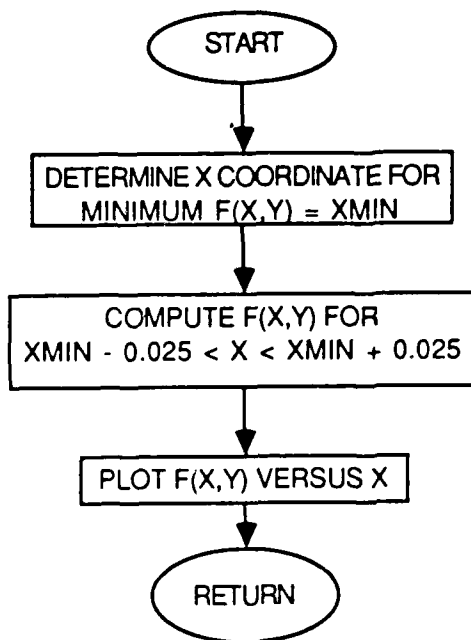


Figure 3.9 Subprogram PLOTTER Flowchart.

The subroutine PLOTTER first computes the minimum value of $F(x,y)$ in the interval $0 < x < 1$ by incrementing x by 0.1 units. This minimum, $XMIN$, is then used as the center of the plot, with $XMIN - 0.025$ and $XMIN + 0.025$ as the lower and upper bounds of the graph. If $XMIN + 0.025 \geq 1.0$ the plot is centered at 0.975 to avoid having the computer attempt to calculate the square root of a negative value of $1 - x^2$ in equation 2.64. After the plot is completed, PLOTTER returns to the program LOCATE.

B. ALGORITHM VALIDATION

1. Generation of Received Signals

The inputs listed in Section A of this chapter for the program LOCATE were generated through the use of two programs. The first program is titled SOUNDRA Y and was written by Professor L. J. Ziomek at the U. S. Naval Postgraduate School, Monterey, California, in 1987. The second program is the subroutine PHSWGT developed by Ziomek and Blount [Ref. 7]. SOUNDRA Y utilizes ray acoustics and geometry to develop feasible geometries for calculations of local angles of arrival of acoustic signals. The inputs to SOUNDRA Y are the X, Y, and Z coordinates of the transmitter, the X and Y coordinates of the receive array, the initial angle of propagation, $\beta(y_T)$, and information describing the local sound-speed profile. SOUNDRA Y then uses equation 2.1 to determine $\beta(y_R)$ and equation 2.15 to calculate ΔR . From this point, geometry alone allows calculation of the RLOS and β LOS, from equations 2.98 and 2.101, respectively, and

$$\Delta Z = (RLOS^2 - \Delta X^2 - \Delta Y^2)^{1/2}. \quad (3.2)$$

In addition, SOUNDRA Y calculates the inputs for the subroutine PHSWGT and the estimates (in this case exact values) of direction cosines for the acoustic signal arriving at the receive array. SOUNDRA Y determines the exact problem geometry, independent of the model-based phase weights, thereby providing the standard by which to judge the solutions generated by the program LOCATE.

2. Test Case Results

a. Double Precision LOCATE versus True Geometry

As stated previously, there are four basic geometries that the program LOCATE is designed to handle. These four geometries may be summarized as:

1. $+\Delta Y, 0^\circ \leq \beta(y_0) < 90^\circ, G > 0.$

2. $-\Delta Y, 90^\circ < \beta(y_0) \leq 180^\circ, G > 0.$
3. $+\Delta Y, 0^\circ \leq \beta(y_0) < 90^\circ, G < 0.$
4. $-\Delta Y, 90^\circ < \beta(y_0) \leq 180^\circ, G < 0.$

Other variations on these geometries are possible by using $-\Delta X$ and $-\Delta Z$, but, because the sound-speed profile is assumed to be a function of depth only, the plane-wave field will propagate in a plane which is normal to the XZ plane [Ref. 1: p. 234]. The result is that variations using $-\Delta X$ and $-\Delta Z$ merely change the sign of the solutions and not the magnitude. LOCATE was written to accommodate $-\Delta X$ and $-\Delta Z$. However, for this discussion, it is sufficient to deal with $+\Delta X$ and $+\Delta Z$ and realize that only the sign of the answer is different when negative quantities are used.

Tables 3, 4, 5, and 6 represent results from the four geometries mentioned above. The sound-speed profile of Figure 2.2 was used in these computations. The value of ΔY for each table was maintained constant and this necessitated the altering of ΔX depending on the angle $\beta(y_0)$ used. If $\beta(y_0)$ was close to 0 degrees or 180 degrees, a smaller ΔX was required than for angles near 90 degrees. This is due to the fact that at angles near 0 degrees or 180 degrees, the plane-wave field reaches depth y_R in a much shorter ΔR than when $\beta(y_0)$ is near 90 degrees. Since from equation 2.99

$$\Delta R^2 = \Delta X^2 + \Delta Z^2, \quad (2.99)$$

ΔX had to be kept sufficiently small to maintain $\Delta Z > 0$, because we are working with cases of positive ΔX and ΔZ .

As can be seen in Tables 3 through 6, the program LOCATE provides excellent results. The slight errors that are present are due mainly to roundoff error occurring in the root finding subroutine ZRPOLY. Note that the constraints concerning turning points have all been observed in these results. The maximum error for any range calculated by LOCATE in these cases was 0.345 meters. The angles calculated by LOCATE are not presented in tabular form because they were all accurate to four significant digits when compared to the true solutions.

Some of the results in Tables 3 through 6 appear to be exact. This is not actually the case because the values in these tables were all rounded to the third decimal place. In no instance were the results of LOCATE exactly equal to the true solution, however, in many instances, the difference was in the fourth or fifth decimal place.

TABLE 3
LOCATE VERSUS TRUE GEOMETRY (GEOMETRY 1)

$\beta(y_0)$	ΔX (m)		ΔY (m)		ΔZ (m)	
	T	L	T	L	T	L
10°	50.000	50.037	300.000	300.000	17.434	17.449
15°	50.000	50.017	300.000	299.999	63.096	63.118
20°	100.000	100.033	300.000	299.999	44.287	44.303
25°	100.000	100.017	300.000	299.999	98.212	98.229
30°	100.000	100.015	300.000	300.000	141.879	141.900
35°	100.000	100.017	300.000	300.000	185.308	185.340
40°	100.000	100.010	300.000	299.999	231.794	231.819
45°	300.000	300.037	300.000	300.000	24.554	24.559
50°	300.000	300.020	300.000	300.000	197.192	197.206
55°	300.000	300.029	300.000	300.000	308.993	309.023
60°	500.000	500.131	300.000	300.001	153.761	153.801
65°	500.000	500.121	300.000	300.001	414.580	414.680
70°	500.000	500.049	300.000	299.976	670.746	670.811
75°	500.000	500.064	300.000	300.001	1035.436	1035.569
80°	500.000	500.038	300.000	300.001	1741.051	1741.185
85°	500.000	500.019	300.000	300.000	5226.883	5227.089

T = true solution L = LOCATE calculation
G = +0.017 sec⁻¹

b. Errors as a Function of Angle of Transmission and/or Depth Separation

(1) *Depth Separation.* Figure 3.10 shows the error in RLOS as the depth separation between the transmitter and the receive array increases, with $\beta(y_0)$ constant. There does not seem to be any relation between the error and the depth separation. The error appears to be mainly caused by roundoff.

(2) *Transmission Angle and/or Depth Separation.* Figure 3.11 shows the error in RLOS as the angle of transmission changes for four different depth separations. Again, it is readily observed that the depth separation has little effect on the size of the error.

TABLE 4
LOCATE VERSUS TRUE GEOMETRY (GEOMETRY 2)

$\beta(y_0)$	ΔX (m)		ΔY (m)		ΔZ (m)	
	T	L	T	L	T	L
95°	500.000	500.060	-300.000	-299.993	2907.664	2908.009
100°	500.000	500.056	-300.000	-299.985	1536.780	1536.952
105°	500.000	500.013	-300.000	-299.976	971.804	971.831
110°	500.000	500.037	-300.000	-300.000	640.734	640.782
115°	500.000	500.052	-300.000	-300.000	395.290	395.332
120°	500.000	500.062	-300.000	-300.000	128.008	128.024
125°	400.000	400.027	-300.000	-300.000	147.308	147.318
130°	300.000	300.129	-300.000	-300.000	191.553	191.637
135°	200.000	200.065	-300.000	-300.000	222.138	111.211
140°	200.000	200.022	-300.000	-300.000	151.643	151.660
145°	200.000	200.051	-300.000	-300.000	62.335	62.353
150°	100.000	100.072	-300.000	-300.000	140.799	140.901
155°	100.000	100.062	-300.000	-300.000	97.297	97.358
160°	100.000	100.066	-300.000	-300.000	43.151	43.182
165°	50.000	50.047	-300.000	-300.000	62.552	62.722
170°	50.000	50.063	-300.000	-300.000	16.779	16.804

T = true solution L = LOCATE calculation

G = +0.017 sec⁻¹

The error does increase as the angle $\beta(y_0)$ is increased above about 60 degrees. This increase can be attributed to the behavior of the sine and cosine functions. Figure 3.12 shows how the sine and cosine functions behave between 0 and 90 degrees. Above about 60 degrees, the slope of the sine function is less than 0.01 degrees⁻¹ so that small changes in the sine cause large differences in the angle $\beta(y)$. Also, in this region the magnitude of the slope of the cosine function is near its maximum. Small changes in the angle $\beta(y)$ create large differences in the cosine.

TABLE 5
LOCATE VERSUS TRUE GEOMETRY (GEOMETRY 3)

$\beta(y_0)$	ΔX (m)		ΔY (m)		ΔZ (m)	
	T	L	T	L	T	L
10°	50.000	49.995	500.000	500.000	72.077	72.071
15°	100.000	99.994	500.000	500.000	88.099	88.094
20°	100.000	99.995	500.000	500.000	150.837	150.830
25°	100.000	100.000	500.000	500.000	209.070	209.067
30°	100.000	99.997	500.000	500.000	268.783	268.777
35°	300.000	300.004	500.000	500.000	175.431	175.434
40°	300.000	300.001	500.000	500.000	288.241	288.243
45°	300.000	300.009	500.000	500.000	393.838	393.850
50°	500.000	500.008	500.000	499.999	310.993	310.999
55°	500.000	500.006	500.000	499.999	494.933	494.940
60°	500.000	499.979	500.000	500.000	686.650	686.620
65°	500.000	499.976	500.000	500.001	916.323	916.279
70°	500.000	499.997	500.000	500.000	1221.188	1221.181
75°	500.000	499.995	500.000	500.000	1671.182	1671.169
80°	500.000	500.002	500.000	499.999	2426.104	2426.112
85°	500.000	500.004	500.000	499.998	3902.854	3902.891

T = true solution L = LOCATE calculation

G = $-0.02956 \text{ sec}^{-1}$

To find ΔY , equation 2.11 uses the roots of equation 2.63 as determined by ZRPOLY. These roots correspond to $\sin \beta(y_0)$. The root contains some small errors due to roundoff which is borne out by the fact that the values of ΔY in Tables 3 through 6 contain errors on the order of 10^{-3} meters. To find ΔR by using equation 2.17, the arc sine of the root must first be calculated. This amplifies any error in the root, especially when the angle is greater than 60 degrees as discussed previously. Next, the cosine of the arc sine of the root is computed, which further amplifies the error.

TABLE 6
LOCATE VERSUS TRUE GEOMETRY (GEOMETRY 4)

$\beta(y_0)$	ΔX (m)		ΔY (m)		ΔZ (m)	
	T	L	T	L	T	L
100°	500.000	499.998	-500.000	-500.000	3539.164	3539.153
105°	500.000	500.000	500.000	-500.000	1966.455	1966.417
110°	500.000	499.983	-500.000	-500.000	1347.650	1347.606
115°	500.000	500.000	-500.000	-500.000	983.983	983.992
120°	500.000	499.986	-500.000	-500.000	728.904	728.884
125°	500.000	499.961	-500.000	-500.000	525.292	525.252
130°	500.000	499.965	-500.000	-500.000	337.478	337.455
135°	500.000	499.980	-500.000	-500.000	71.388	71.389
140°	300.000	299.990	-500.000	-500.000	298.440	298.432
145°	300.000	299.979	-500.000	-500.000	185.560	185.548
150°	100.000	99.991	-500.000	-500.000	272.886	272.863
155°	100.000	99.987	-500.000	-500.000	212.229	212.201
160°	100.000	99.990	-500.000	-500.000	153.303	153.288
165°	100.000	99.974	-500.000	-500.000	90.286	90.264
170°	50.000	49.978	-500.000	-500.000	73.210	73.181

T = true solution L = LOCATE calculation
G = -0.02956 sec⁻¹

Therefore, above about 60 degrees, we see these increased errors manifest themselves in the ΔR , ΔX , ΔZ , and RLOS calculations. Still, the errors seen in Figure 3.11 and in Tables 3 through 6 are insignificant when compared with the ranges in question. The angles are still accurate to four significant digits, and consequently, the range errors remain small.

c. Double Precision Versus Single Precision Results

It was found that the single precision version of ZRPOLY was not accurate enough to calculate the correct answers. The reason for this can be seen in Table 7 which contains some single precision results for comparison to double precision results. ZRPOLY calculates the roots shown in the two right hand columns of Table 7. Even

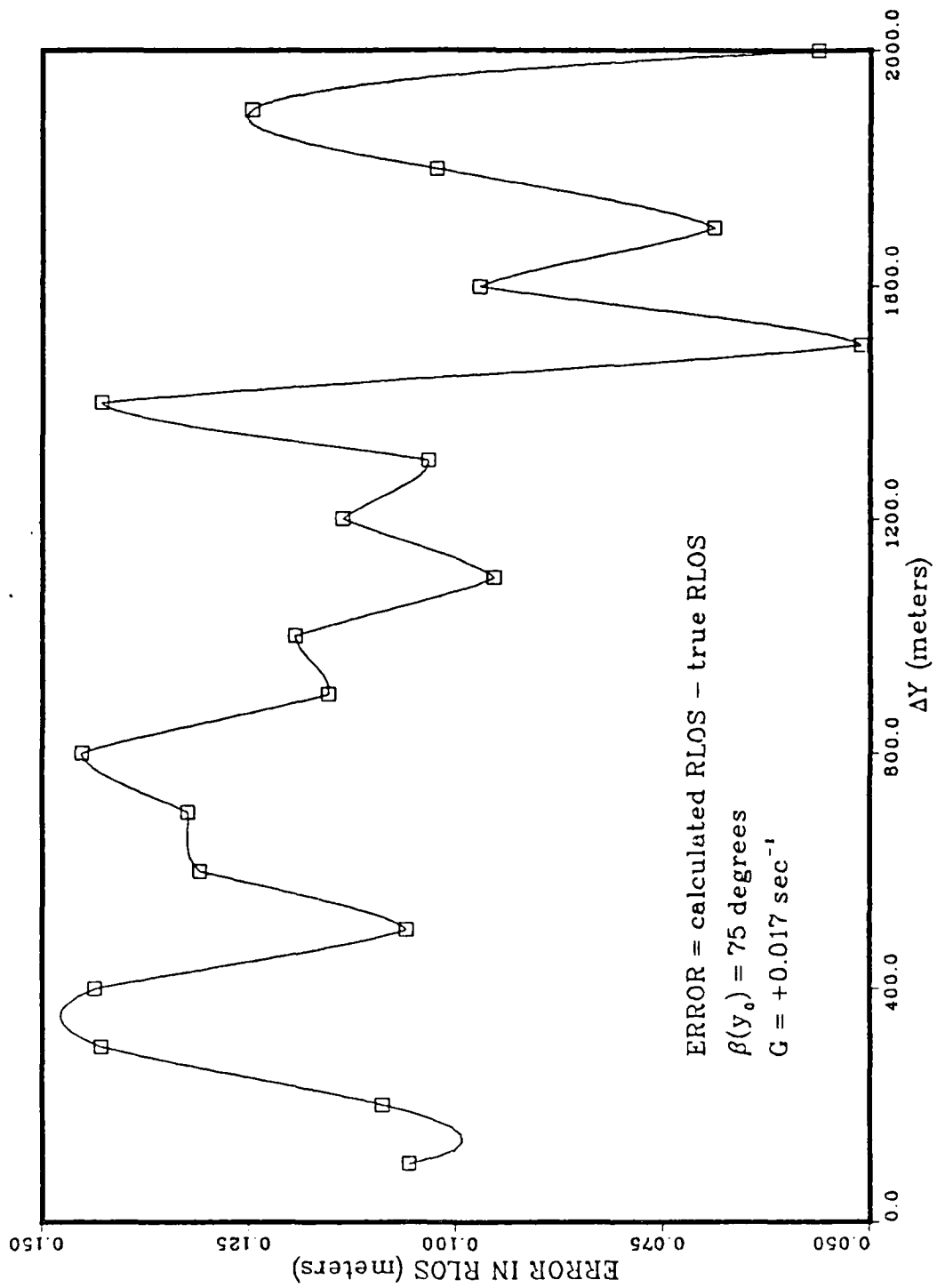


Figure 3.10 Error in RLOS as a Function of Depth Separation.

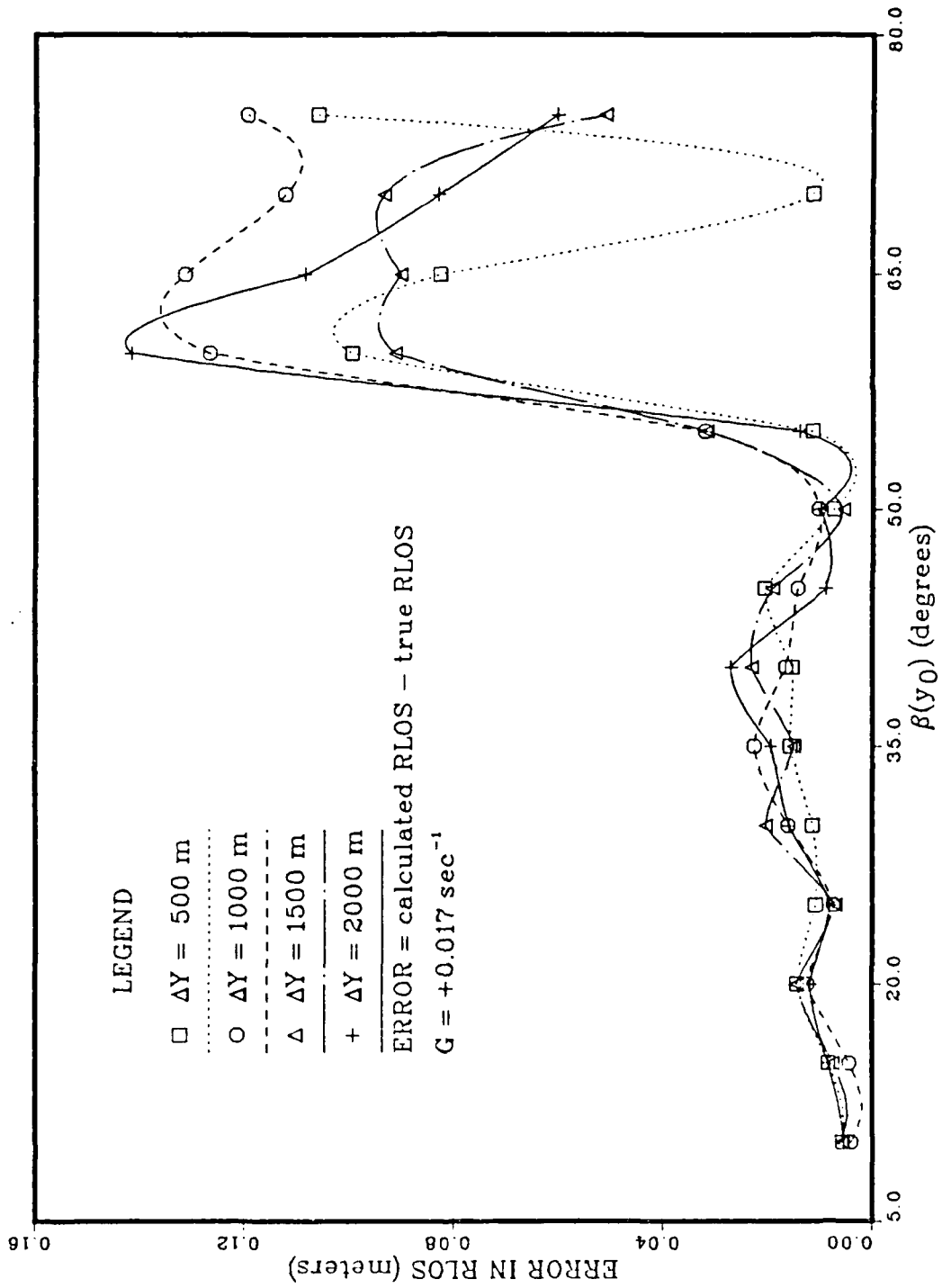


Figure 3.11 Error in RLOS as a function of Transmission Angle and or Depth Separation.

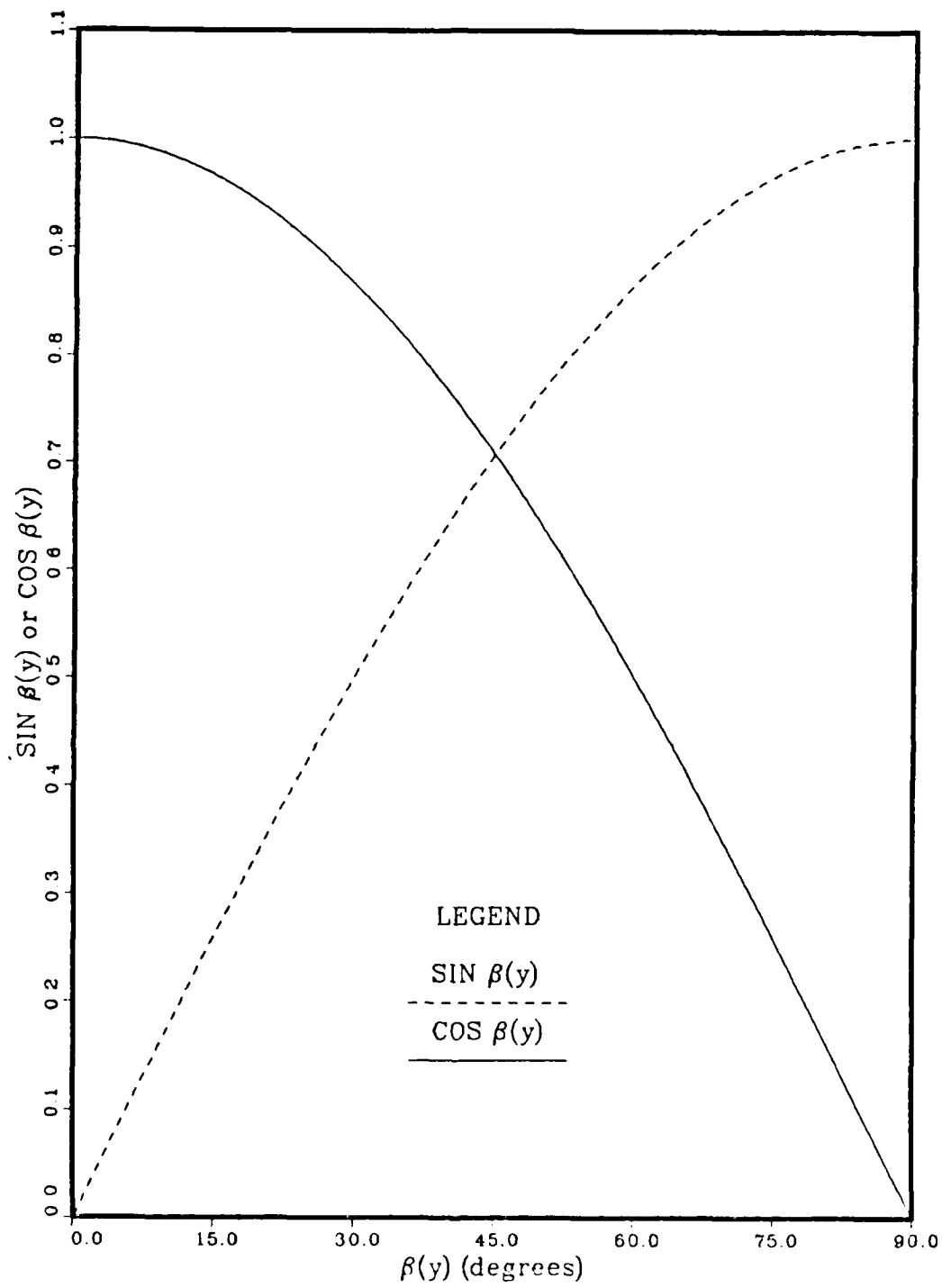


Figure 3.12 Sine and Cosine for 0 to 90 Degrees.

TABLE 7
DOUBLE PRECISION VERSUS SINGLE PRECISION RESULTS

DP	SP	DP	SP	DP	SP
$\beta(y_0)$	$\beta(y_0)$	RLOS (m)	RLOS (m)	Root	Root
60.17°	60.41°	603.147	9.264	0.8660	0.8689
65.21°	65.44°	715.599	48.291	0.9063	0.9092
70.28°	70.58°	888.832	28.699	0.9397	0.9428
75.38°	75.75°	1188.473	30.835	0.9659	0.9693
80.60°	81.18°	1836.237	57.808	0.9912	0.9881
86.73°	88.34°	5259.514	350.602	0.9961	0.9997

$G = +0.017 \text{ sec}^{-1}$

though the roots appear accurate to the second significant digit in the single precision results, when dealing with sines and cosines, an error in the third significant digit can create a fairly large error in calculating the angle $\beta(y_0)$. Also, these roots are multiplied by the radius of curvature, a , in equation 2.11. This radius of curvature is on the order of 10^5 meters, so small errors in the roots will create large errors in the ranges calculated. The single precision results in Table 7 are so poor that they seem to have no relation to the actual answer. The double precision results for RLOS in Table 7 are accurate to within 0.1 meters of the true solution.

IV. CONCLUSIONS AND RECOMMENDATIONS

The goal of this thesis was to determine if an underwater acoustic transmitter can be localized using ray acoustics, model-based phase weights, estimates of the local angles of arrival, and knowledge of the local sound-speed profile. As demonstrated in Chapter III, this goal is achievable and to a high degree of accuracy depending on the accuracy of the inputs to LOCATE. There are restrictions on the use of this procedure. It appears that the restrictions do not impose severe limitations on the use of the algorithm, and in some cases it may be possible to overcome them altogether.

All the restrictions basically result in a limitation on the effective range of the algorithm. Even though acoustic signals may not reach their initial turning points for theoretical ranges in the tens or even hundreds of kilometers, the ocean is only about 11.5 kilometers deep at its greatest depth. Therefore, the ranges shown in Table I are not realizable in some cases because the signal will reach the ocean floor in less range than it would take to reach the turning point. Additionally, underwater acoustic transmitters are usually limited in the depth to which they may be deployed, so that the angles of transmission that are associated with the greatest ranges will pass well below the receive array at any significant range. Still, the algorithm appears to be quite useable in ranges of less than 10 kilometers. This would be of a great advantage in the case of a transmitter whose signal is of low power, resulting in a short detection range. In fact, the need for an algorithm of this sort is most critical when the transmitter is at short range and its exact location and direction of motion must be resolved rapidly.

In some instances, the limitations due to turning points may not be of much concern. For example, the algorithm might be used for an array located on the ocean floor. In this case, much longer ranges would be achievable, provided that the transmitter is in the same portion of the sound-speed profile as the receive array. The algorithm might also be of use in active sonar systems to provide more accurate range and depth information than is currently available.

Implementation of the algorithm must include a very accurate root finding technique as has been discussed. Due to the sensitivity of the problem in regard to the sine and cosine functions, the roots need to be accurate to at least three significant figures. It was found that this is only possible through use of a double precision root finding subroutine. This, of course, causes the program to run more slowly but,

because the remainder of the program can still be written in single precision, it is not a great hinderance.

In the future some areas requiring more study are:

- Develop a method for obtaining the model-based phase weights from the received signals. At present, phase weights are computed based on received signals, however, the phase weights in the Y direction need to be separated into traditional phase weights and model-based phase weights.
- Determine a method to account for the acoustic signal passing through a turning point prior to reaching the receive array. This would greatly extend the range capability of the algorithm.
- Develop methods to identify signals that are transmitted from portions of the sound-speed profile other than the gradient in which the receive array is located.
- Investigate the practical applications of the algorithm in varying acoustic conditions, particularly in regions such as near the Gulf Stream where the sound-speed profile is a function of depth and range.

LIST OF REFERENCES

1. Ziomek, L. J., *Underwater Acoustics — A Linear Systems Theory Approach*, Academic Press, Inc., 1985.
2. Ziomek, L. J., and Chan, F., "Frequency Domain Adaptive Beamforming for Planar Arrays," *Conference Record Twentieth Asilomar Conference on Signals, Systems, and Computers*, pp. 120-124, Pacific Grove, California, 10-12 November 1986.
3. Ziomek, L. J. and Blount, R. J. Jr., "Underwater Acoustic Model — Based Signal Processing," *IEEE Transactions Acoustics, Speech, Signal Processing*, accepted for publication, scheduled to appear in the December 1987 issue.
4. Flatte', S. M., ed., *Sound Transmission Through a Fluctuating Ocean*, Cambridge University Press, 1979.
5. Kinsler, L. E., and others, *Fundamentals of Acoustics*, 3rd ed., John Wiley & Sons, Inc., 1982.
6. Brekhovskikh, L. M., and Lysanov, Y., *Fundamentals of Ocean Acoustics*, Springer — Verlag, 1982.
7. Blount, R. J., Jr., *Underwater Acoustic Model — Based Signal Processing Applied to the Detection of Signals from a Planar Array of Point Source Elements*, Master's Thesis, Naval Postgraduate School, Monterey, California, September, 1985.

INITIAL DISTRIBUTION LIST

	No. Copies
1. Defense Technical Information Center Cameron Station Alexandria, VA 22304-6145	2
2. Library, Code 0142 Naval Postgraduate School Monterey, CA 93943-5002	2
3. Professor L. J. Ziomek, Code 62Zm Department of Electrical and Computer Engineering Naval Postgraduate School Monterey, CA 93943-5000	3
4. Professor J. P. Powers, Code 62Po Department of Electrical and Computer Engineering Naval Postgraduate School Monterey, CA 93943-5000	1
5. LT M. D. Budney Naval Submarine School Code 20 SOAC 88030 Box 700 Groton, CT 06349	1
6. Chief of Naval Operations Code OP-02 Navy Department Washington, D.C. 20350	1
7. Dr. Duncan Sheldon (Surface Sonar) NUSC Code 3314 New London, CT 06320	1

END

DATE

FILMED

5-88

DTIC